



Site Effects Assessment Using Ambient Excitations

**European Commission – Research General Directorate
Project No. EVG1-CT-2000-00026 SESAME**

**Report on
Simulation for real sites**

WP10

**Set of noise synthetics for H/V and array studies from
simulation of real sites and comparison for test sites**

Deliverables D11.10 and D17.10

December 2004

List of contributors

(in alphabetical order after the last name)

Julien Banton	LGIT, Grenoble, France
Pierre-Yves Bard	LGIT, Grenoble, France
Sylvette Bonnefoy-Claudet	LGIT, Grenoble, France
Cécile Cornou	ETHZ, Zürich, Switzerland
Giuseppe Di Giulio	INGV, Roma, Italy
Donat Fäh	ETHZ, Zürich, Switzerland
Philippe Guéguen	LGIT, Grenoble, France
Bertrand Guillier	LGIT, Grenoble, France
Fortunat Kind	ETHZ, Zürich, Switzerland
Jozef Kristek	GPI-SAS, Bratislava, Slovakia
Peter Moczo	GPI-SAS, Bratislava, Slovakia
Matthias Orhnberger	IGUP, Potsdam, Germany
Antonio Rovelli	INGV, Roma, Italy
Estelle Schissel�-Rebel	IGUP, Potsdam, Germany
Frank Scherbaum	IGUP, Potsdam, Germany
Marc Wathelet	GEOMAC, Liege, Belgium
Daniel Vollmer	IGUP, Potsdam, Germany
Project coordinator:	Pierre-Yves Bard
Task C leader:	Pierre-Yves Bard
WP10 leader:	Donat F�h

Summary

In the following we report the results of the ambient noise modelling for real sites. This work was conducted under the framework of the SESAME Project (Site Effects Assessment Using Ambient Excitations, EC-RGD, Project No. EVG1-CT-2000-00026 SESAME), Task C (physical background and noise simulation), Work Package 10 (WP10 – Simulation for real sites)

List of contents

1	Introduction.....	5
2	Ambient noise simulation.....	6
3	Colfiorito basin.....	6
3.1	Geophysical model	6
	Geometry of the model	6
	Geophysical parameters	8
3.2	H/V and array experiments.....	9
3.3	Noise simulation	10
4	Geophysical model of the Grenoble basin	12
4.1	Geophysical model	12
4.2	H/V and array experiment	16
4.3	Noise simulation	19
5	Geophysical model of the Basel area	21
5.1	Geophysical parameters	21
	Geometry of the model	21
	Geophysical parameters	23
	Refinement of the model geometry with H/V polarization	25
5.2	H/V and array experiment	30
5.3	Noise simulation	32
6	Comparison between real and synthetics noise data: example of Grenoble and Colfiorito basins.....	36
6.1	H/V, array analysis and inverted seismic profiles.....	36
6.2	H/V and array techniques on simulated noise.....	37
	H/V technique	37
	Array technique.....	39
6.3	Comparison with the actual ambient noise	48
	Colfiorito basin	48
	Grenoble basin	51
7	Conclusion	54

8	Waveform data description	55
9	Acknowledgments	55
10	References.....	56
11	List of Figures	59
12	List of Tables	62

1 Introduction

The analysis of ambient vibration recordings for site effect estimation has gained more and more interest in recent years. It is indeed commonly thought that both single station methods (H/V technique after Nakamura, 1989) as well as array measurements (Tokimatsu, 1997) may allow to obtain estimates of the fundamental resonance frequency (H/V technique) and the shallow shear velocity profiles at a given array location. Considering that such field experiments are inexpensive and do not require heavy seismic sources or drilling, the passive recording of ambient vibrations may provide a low-cost mapping tool of site features even in urban areas, where geotechnical information is usually difficult to obtain. However, physical basis and actual relevancy of such methods for site effect estimates have never reached a scientific overall agreement. Numerical simulations of the noise wave field and cross checking of observations, numerical simulations and known structure for a few well-known test-sites should also help in investigating the reliability of these techniques to retrieve relevant information for site effect estimation, whatever the structure (1D, 2D or 3D). Within this project, we have simulated ambient noise for the shallow sedimentary basin of Colfiorio (Italy), the deep sedimentary basins of Grenoble (French Alps) and Basel (Switzerland). The structure of these sites is well known and array ambient vibrations have already been performed in the past or within this project (SESAME Deliverable D06.05).

We first describe the ambient noise modeling procedure, the geophysical settings of the three test sites as well as the H/V and array measurements campaign that were performed and the parameters used for the noise modeling. Then, for Colfiorito and Grenoble sites, the simulated ambient noise and the known structure are compared in terms of fundamental resonance frequency and inverted velocity profiles at array sites that were actually deployed in the field. Next, synthetics and actual noise are compared at these array sites in terms of inverted seismic profiles and resonance frequencies. These comparisons should finally help in answering the following questions: is the ambient noise modeling procedure used here able to capture the actual noise wave field? Do the H/V and array techniques provide relevant information about the site features?

2 Ambient noise simulation

The numerical code ("FD code to generate noise synthetics", SESAME Deliverable D02.09) that has been developed within this project is used to simulate ambient noise originated by human activity, for sites with heterogeneous subsurface structures. Ambient noise simulations performed for 1D models using different sources at different depths and spatial location have shown that local surface sources are appropriate for getting a good representation of the actual noise in terms of both H/V and measured dispersion curves through array processing (Bonnetfoy-Claudet et al., 2004; SESAME Deliverable D13.08). For the modeling of real sites, noise sources were thus approximated by surface or subsurface forces, distributed randomly in space and time, with random direction (vertical or horizontal) and amplitude. The time function is either a delta-like signal (impulsive sources) or a pseudo-monochromatic signal ("machine" sources) (a harmonic carrier with the Gaussian envelope). Computation of the associated wave field is performed using an explicit heterogeneous 3D finite-difference scheme solving equations of motion in the heterogeneous visco-elastic medium with material discontinuities.

3 Colfiorito basin

3.1 Geophysical model

The description of the Colfiorito model given here relies mainly on the work of Rovelli et al. (2001) and Di Giulio et al. (2003).

Geometry of the model

The Colfiorito plain is an approximately 3-km wide intermountain basin in the southern part of the northern Apennine arc, a classic fold and thrust belt (Bally et al., 1986). The Umbria-Marche belt was formed during Late Miocene-Middle Pliocene times and subsequently has been affected by extensional tectonics. The origin and the evolution of the main intermountain basins in northern and central Apennines are attributed to this extensional phase (Calamita et al., 1994) or to younger transtensional faulting (Cello et al., 1997).

The structural depression of Colfiorito is filled with Quaternary alluvial deposits composed of lateral debris fans interfingering with the lacustrine sandy-clayey deposits that constitute the main body of the sedimentary fill. These soft sediments overlie a rock basement of limestones

and marls of the Umbria-Marche Meso-Cenozoic Sequence. Seismic and geoelectric surveys were made to reconstruct the buried interface between low- and high-velocity layers. An E-W seismic refraction profile along with seven shorter transect at the margins of the basin were performed for a total extension of 960 m. Seismic data were integrated with seven geoelectric lines for a total extension of 10,400 m obtained through 84 vertical geoelectric soundings and with a 630-m long multielectrodes profile (Figure 1). A joint approach using geophysical, geologic, and geomorphic data was adopted to image the interface between the main low- (silty-clayey sediments) and high-velocity (carbonate bedrock and/or sandy-pebbly conglomerate) layers within the Colfiorito basin. The dataset includes a total of 1,186 elevation points of the high-velocity layer, subdivided into the following groups: 132 points estimated through geophysical (seismic and geoelectric) surveys; 13 points taken from borehole and electric logs from Messina et al. (2002) at locations of poor coverage of our surveys; 50 points for which the elevation of bedrock was inferred from geomorphic interpretation of either the basin walls or thalwegs of tributary streams; 168 points almost evenly distributed along the infill boundary; 823 points collected within a 100-500 m wide band around the edge of the basin. These scattered data points were grided through a Triangular Irregular Network interpolation method (Akima, 1978) using a quintic polynomial surface which honors the data values and predicts some degree of over- and under-estimation above and below local high and low data values. The ground surface elevation of every data point was obtained through a digital terrain model with a cell size of 20 m.

Figure 1 shows a contouring display of the grided thickness of the low-velocity layer within the basin and the topography of surrounding uplands. Several narrow and deep sub-basins can be observed within the plain; the deepest ones (up to about 180 and 150 m) are located at the NW corner of the basin. A relatively flat and shallower (60-70 m) area occupies the center of the basin. The geometry of the western basin wall mimics quite well the dip of a N-S trending anticline forelimb, and the northeastern wall partly follows the NW-SE trend of normal faults (according to the structural sketches by Cinti et al., 2000, and Mirabella and Pucci, 2002). The irregular shape of the interface between the low-velocity layer and the bedrock (carbonates and conglomerates) could have been originated from karstic processes as suggested by several sink-holes, dolines and other karstic landforms that are widespread in the area. However, the presence of normal faults, and their associated damaged-rock zone, on the NE wall of the basin implies a possible role of tectonics in favoring rock weakness beneath the basin along the NW-SE direction.

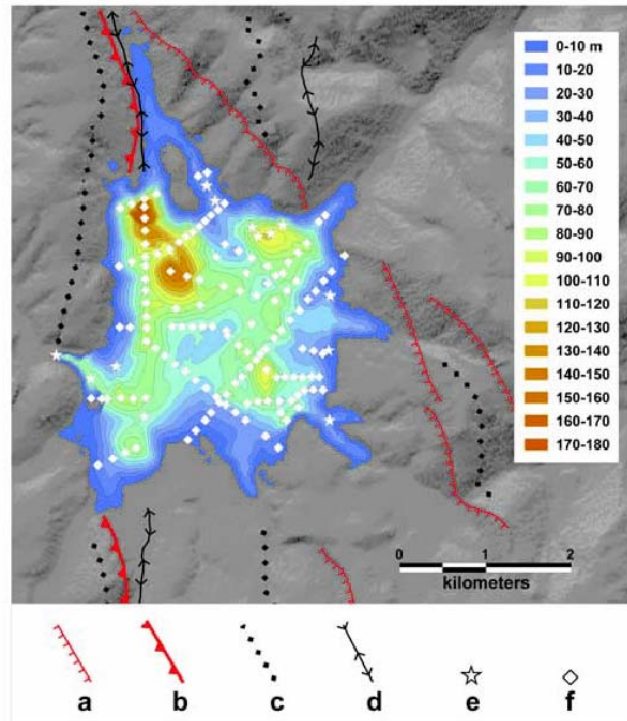


Figure 1: Thickness of the low-velocity layer in map view. (a) normal faults; (b) thrust faults; (c) anticline axes; (d) syncline axes; (e) borehole location; (f) geophysical survey lines. After Di Giulio et al. [2003]

Geophysical parameters

Studies performed in the central part of the basin by Di Giulio et al. (2003) and Rovelli et al. (2001) have allowed to constrain the S-wave velocities and the attenuation values within the sediments and rock basement: the S-wave velocities are about 200 m/s and 1200 m/s for the sediments and the rock basement, respectively, while the quality factor is 40 for both P- and S-waves within the sediments. The low S-wave velocity was recently confirmed (A. Rovelli, *personal communication*) by the drilling of a borehole that allowed *in situ* compressional- and shear-wave measurements (Figure 2).

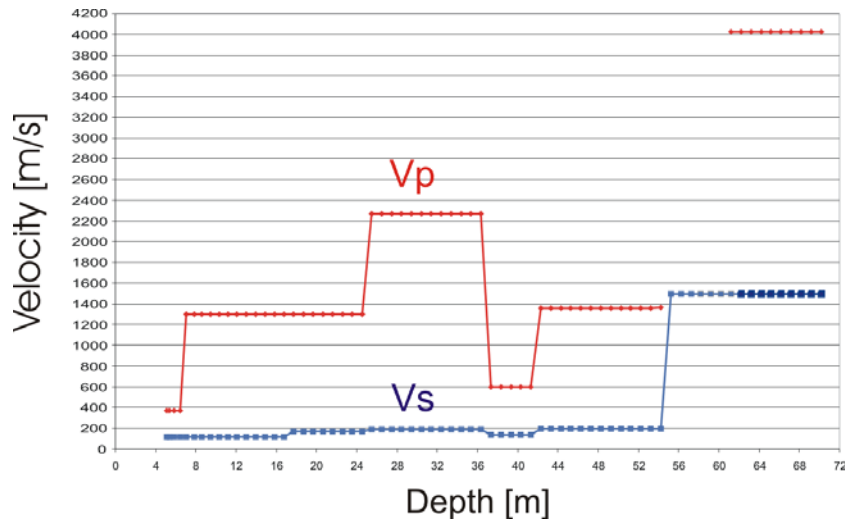


Figure 2: P- and S- wave velocities derived from down-hole measurements [A. Rovelli, *personal communication*]

3.2 H/V and array experiments

Within the SESAME project, some array measurements have been performed in July 2002. All the information regarding these measurements may be found in the SESAME Deliverable D06.05 “Array data set for different sites”. Arrays distribution and geometry within the Colfiorito basin are displayed in Figure 3.

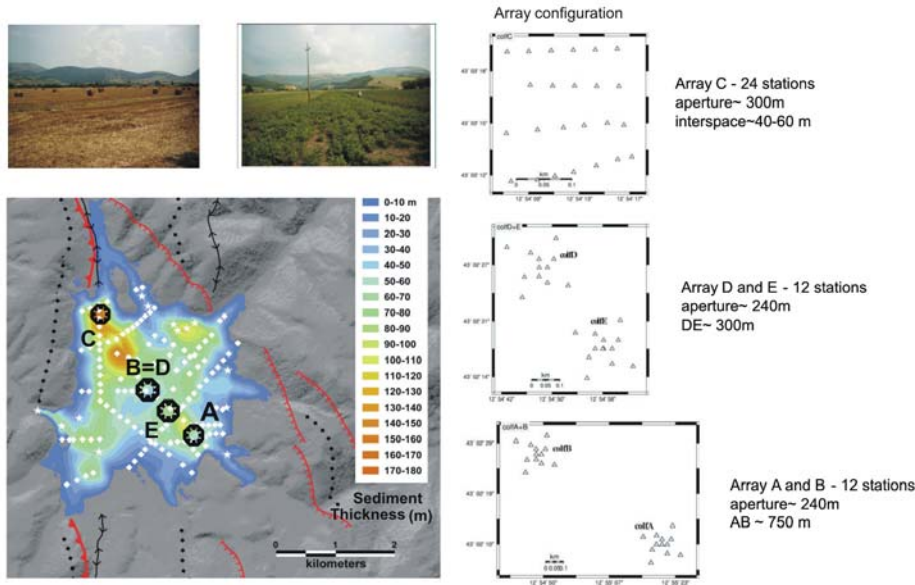


Figure 3: Arrays distribution within the Colfiorito basin (left panel) and configuration of the arrays (right panel) deployed during the 2002 measurement campaign.

3.3 Noise simulation

The geophysical parameters used for the FD noise simulation are indicated in Table 1. The geophysical parameters used for the FD noise simulation are indicated in Table 1. We have considered 346 receivers (Figure 4) located at the free surface, some of them fitting the real noise array measurement locations. Sources composed of 50% of delta-like and 50% of pseudo-monochromatic signals have been randomly distributed at the free surface within the basin. Two computations have been performed involving different number of sources (Table 2). Besides, in order to limit the total CPU time, simulations were performed for two distinct frequency bands: from 0.3 to 1.6 Hz and from 1.3 to 3.3 Hz. This 0.3-3.3 Hz frequency range includes most of the frequencies that were amplified during last 1997 Umbria Marche seismic sequence (Di Giulio et al., 2003). The main parameters used for the FD simulation (grid spacing, frequency band, size of the finer and coarser FD grids) are indicated in Table 3.

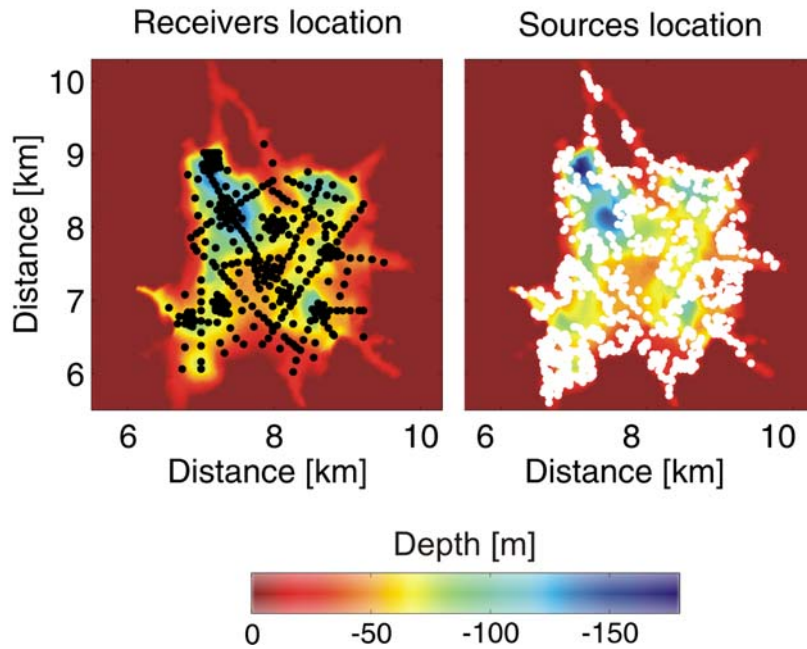


Figure 4: Topography of the low-velocity layer, with the receivers (black dots) and the sources (white dots) locations.

Table 1: Geophysical parameters of the Colfiorito basin considered for the noise simulation

	Vp [m/s]	Vs [m/s]	Qp	Qs	ρ [kg/m ³]
sediments	800	200	40	40	1900
bedrock	$2.24z^{(*)}+2200$ $z<1000$ m	$1.2944z^{(*)}+1200$ $z<1000$ m	200	200	$0.2z^{(*)}+2300$ $z<1000$ m
	4400 $z>1000$ m	2494.4 $z>1000$ m			2500 $z>1000$ m

Commentaire : dddd

(*) z is depth in meters

Table 2: Noise simulation performed for the Colfiorito basin

Dataset#	Duration [s] and frequency range	Number of sources	Comments
1003	198 [0.3 1.6 Hz]	1688	Sources located at the surface within the sediment fill
	198 [1.3 3.3 Hz]	1688	
1004	208 [0.3 1.6 Hz]	1022	Sources located at the surface within the sediment fill
	163 [1.3 3.3 Hz]	801	

Table 3: Computation parameters used for Colfiorito model

Freq. Range [Hz]	Finer grid				Coarser grid				Sampli ng rate (s)
	Grid spacing [m]	X [m]	Y [m]	Z [m]	Grid spacing [m]	X [m]	Y [m]	Z [m]	
0.3 – 1.6	20	16140	16140	320	60	16140	16140	17340	0.0032
1.3 – 3.3	10	5550	4770	310	30	5550	4770	4170	0.0016

4 Geophysical model of the Grenoble basin

The description of the Grenoble model given here relies mainly on the work of Lebrun (1997), Vallon (1999) and Cornou (2002).

4.1 Geophysical model

The Grenoble basin displayed in Figure 5 is a 3D Y-shaped deep basin filled mostly with late-Quaternary postglacial deposits overlaying Jurassic marls and a marly limestone substratum. A deep borehole (Figure 5) drilled by the Institut de Radio-protection et de Sûreté Nucléaire (www.irsn.fr) in the northeast branch of the valley hit the substratum at 532-m depth (Lemeille *et al.*, 2000, Nicoud *et al.*, 2002). Bouguer anomaly analysis of 10 years of gravity measurements (Vallon, 1999) provided the substratum topography (Figure 6) that fits at the borehole location the substratum depth evaluated through seismic and borehole measurements (Nicoud *et al.*, 2002, Cornou, 2002). Logging operations performed in the borehole, as well as the investigation of contribution of vertical and offset seismic profiles (Figure 7), show that the *P*-wave velocity varies between 1500 and 2150 m/sec and the *S*-wave velocity between 250 and 950 m/sec from the surface down to the bedrock (Cornou, 2002). *In situ* borehole measurements at 550-m depth have indicated a *P*-wave velocity of 4500 m/sec within the bedrock, whereas the seismic refraction profile has provided a *P*-wave propagating at 5600 m/sec at the top of the bedrock (Cornou, 2002). In the following we will consider a *P*-wave velocity of 5600 m/sec in the substratum that leads to an *S*-wave velocity of 3200 m/sec assuming a Poisson coefficient of 0.25 in the substratum. Seismic velocity profiles are displayed in Figure 5b. The *S*-wave velocity profile exhibits a low velocity value (250 m/sec) within a 40-m-thick surficial layer that leads to an *S*-wave velocity contrast of about 2 with the layer underneath. This relatively low *S*-wave topmost layer was very recently confirmed by a second borehole drilled near the previous one: cuttings have thus shown a major sand/marl contrast at 40-m depth (F. Lemeille, *personal communication*). Besides these measurements,

Lebrun *et al.* (2001) conducted a horizontal/vertical (H/V) microzonation study within the area of Grenoble. They observed a resonance frequency of 0.3 Hz in the central part of the basin and another one, in some parts of the city, near 3 Hz that they assigned to the resonance frequency of a very surficial layer. The spatial distribution of fundamental frequency values over the whole basin agrees with the gravimetric model when assuming a mean *S*-wave velocity of about 700 m/sec (Lebrun, 1997). Moreover, attenuation values have been measured within the frequency range 15–40 Hz and were found to be rather stable over the whole sediment thickness with a quality factor of about 40 and 20 for *P*- and *S* seismic waves, respectively (Cornou, 2002).

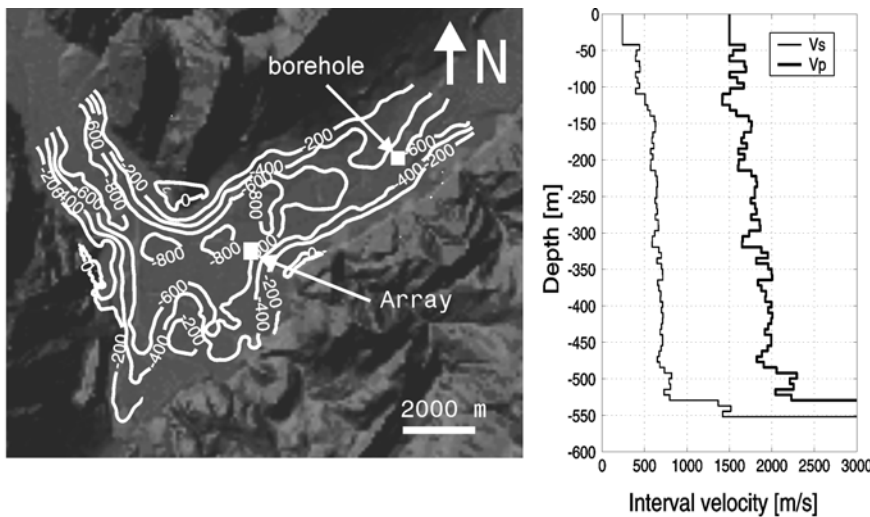


Figure 5: a) Grenoble basin's digital elevation model and, superimposed, the 3D contour map of the basement's depth (white lines) inferred from gravimetric measurements (Vallon, 1999). Depth is given in meters. Location of the array and the borehole are also indicated. b) P- (thick line) and S- (thin line) wave interval velocity profiles derived from vertical and offset seismic profiles measurements at the borehole location (Cornou, 2002).

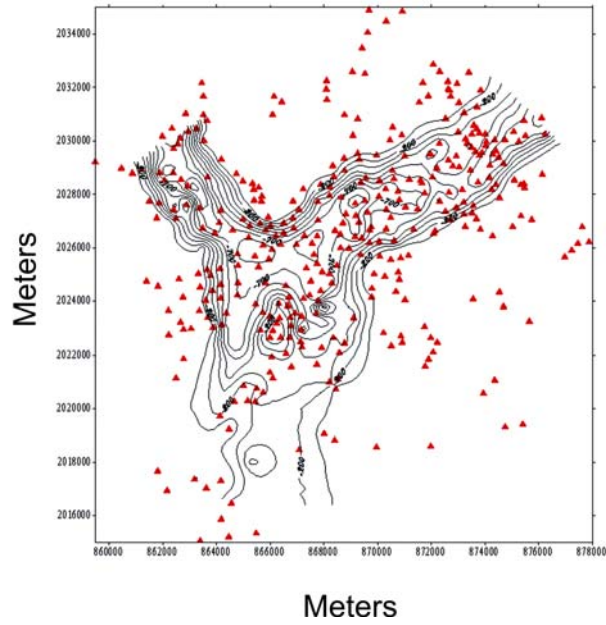


Figure 6: Contour map of the basement's depth (black lines) inferred from gravimetric measurements (red triangles). After Vallon (1999)

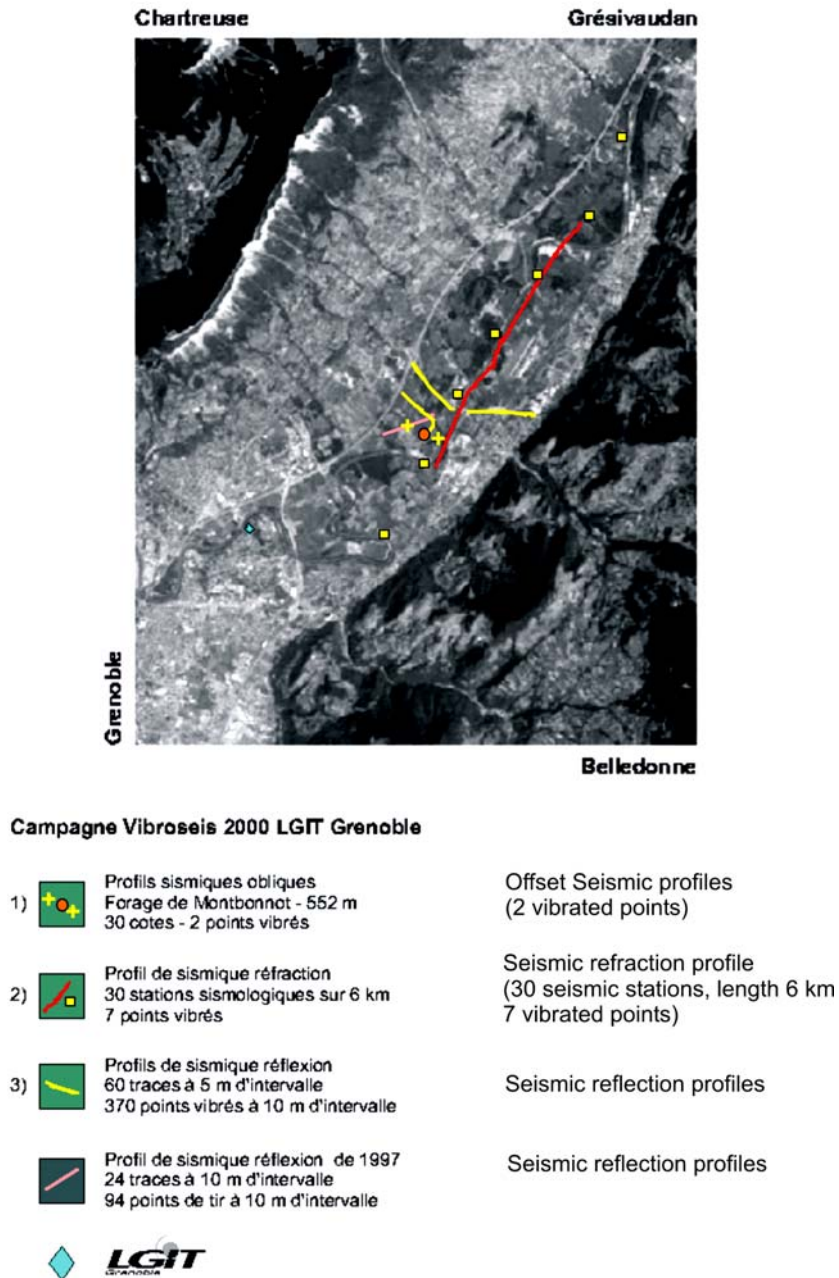


Figure 7: Seismic profiles (Vertical and offset seismic profiles, seismic refraction and reflection profiles) performed nearby the borehole location (after Cornou, 2002)

4.2 H/V and array experiment

Several array measurements were carried out in the past within the Grenoble basin:

- a noise array measurements campaign at eight different sites was conducted during april 1999 (Scherbaum et al., 1999; Bettig et al., 2001) Arrays distribution and geometry within the city are indicated in Figure 8. These measurements were performed using Lennartz 5s seismometers connected to MarsLite acquisition systems. At each site, the measurements lasted for at least three hours.
- an array involving 29 three-component seismic sensors was installed approximately at the same location as array G in Figure 8 and operated from February to May 1999. Dedicated to earthquake recordings for site effects purposes (Cornou et al, 2003), sensors were arranged in concentric rings: 16 L22 Mark Products sensors (with a flat response between 2 and 50 Hz) were located in two inner rings with a maximum 80 m aperture, 12 wider band sensors (3 Lennartz Le3D-5s and 9 Guralp CMG40-20s, with a flat response from 0.2 and 0.05 to 50 Hz, respectively) were installed in a maximum 1 km aperture outer ring and one CMG40-20s sensor added at the center of the array. Sensor locations were precisely determined using static GPS measurements (precision of about 0.3 m). Sensors were connected either to Reftek-72A2 or to a Minititan-3XT recorder. Data were continuously recorded, time synchronization was provided by continuous GPS receivers (time accuracy less than 1 ms) and the sampling rate was fixed to 125 Hz on each channel.

Some extensive H/V noise measurements have been performed in 1997 by Lebrun et al. (2001). However, a new H/V campaign involving 15 minutes of noise recordings was very recently carried out at 294 measured sites (Benton, 2004) (Figure 10).

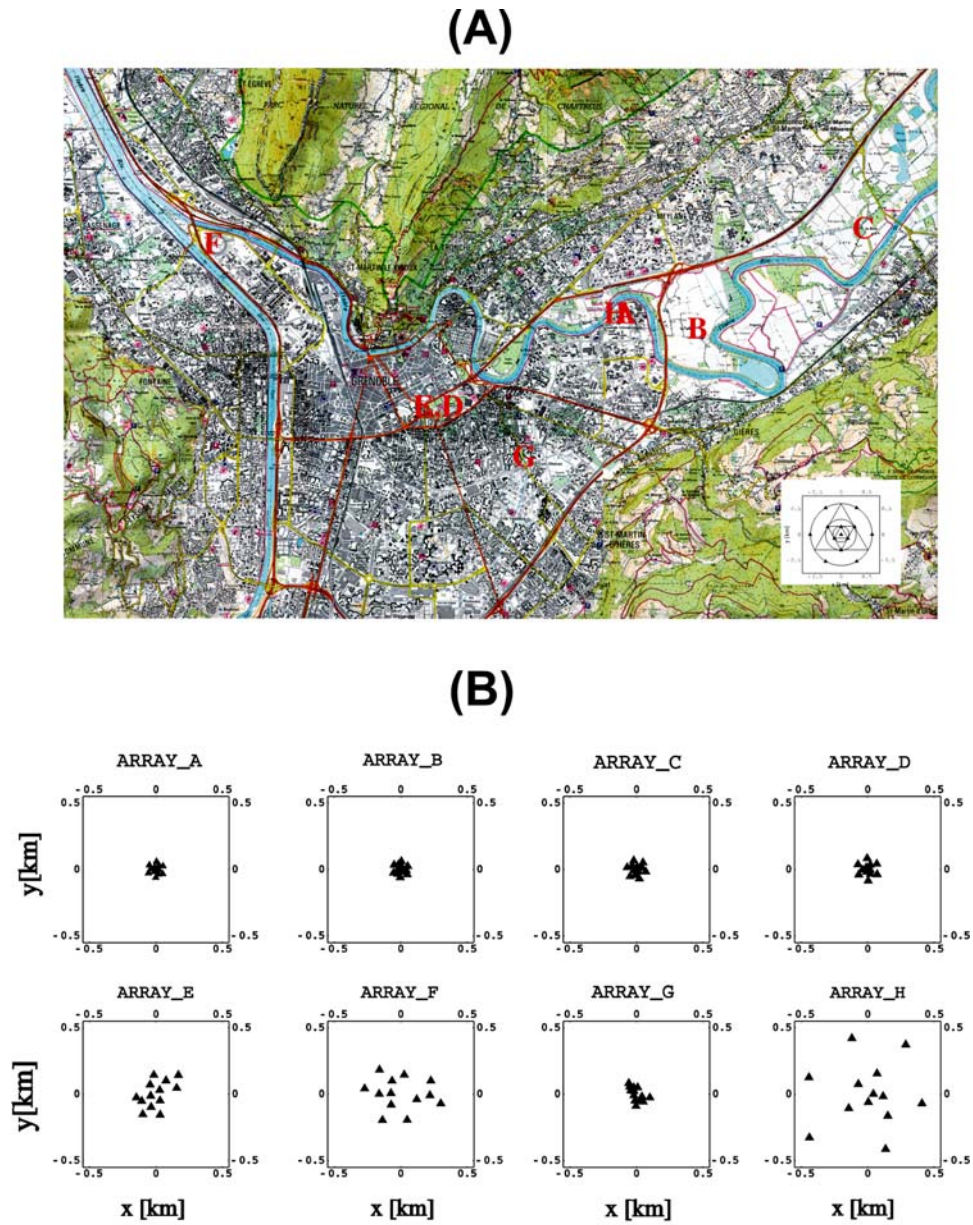


Figure 8: (A) Array distribution within the city of Grenoble. The array locations are denoted by letters A-I. Arrays A and H as well as E and D occupied nearly the same locations with different apertures. (B) Array design. Apertures: A: 121 m; B : 122 m ; C : 143 m ; D : 169 m ; F : 584 m ; G : 192 m ; H : 1001 m. After Scherbaum et al. (1999).

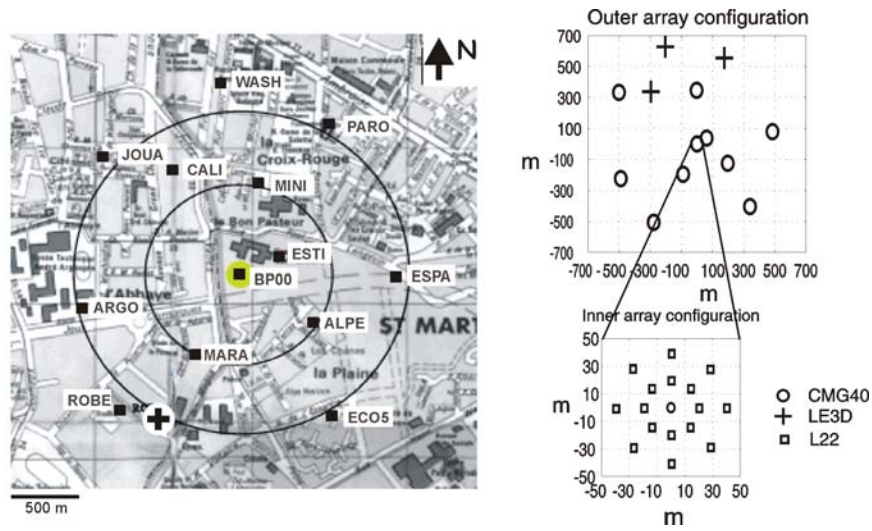


Figure 9: (left) Approximative geographical array location. (right) Outer and inner array configuration. The BP00 station is located at the center of the inner array.

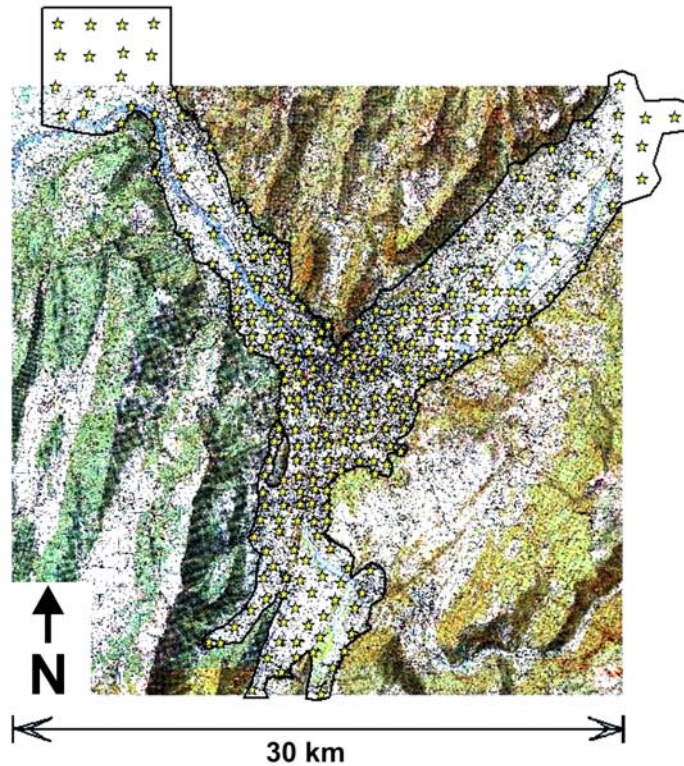


Figure 10: 2004 H/V noise measurements campaign. Measured points are indicated by the yellow star. After Benton (2004).

4.3 Noise simulation

The geophysical parameters used for the noise modeling are indicated in Table 4, where the P- and S-wave velocity profiles measured at the borehole location were extrapolated using gradient functions up to 800 m¹ (Figure 11). Noise has been simulated within the 0.2 to 1.1 Hz frequency band that corresponds to the lowest part of the actually amplified frequency band, from 0.2 to 10 Hz (Lebrun et al., 2001). 1273 receivers have been distributed at the free surface (Figure 12), some of them fitting the real noise array measurements locations. Sources composed of 50% of delta-like and 50% of pseudo-monochromatic signals have been randomly distributed at the free surface within the basin. Two computations with a different number of sources have been performed (Table 6). The main parameters used for the FD simulation (grid spacing, frequency bands, size of the finer and coarser FD grids) are indicated in Table 5.

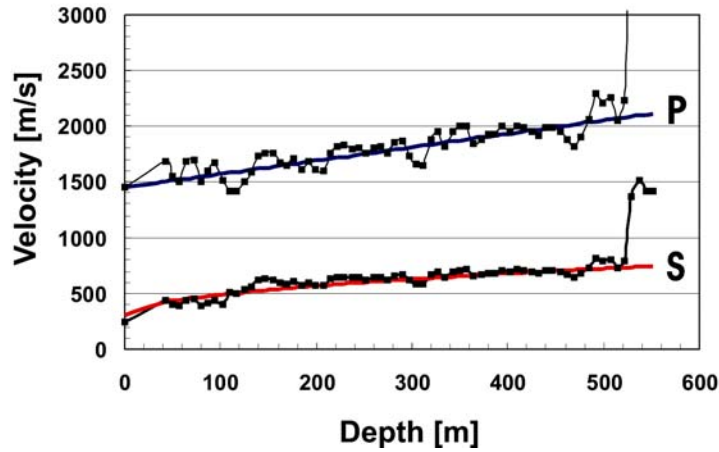


Figure 11: Interval P- and S- wave velocity (black squares) at the borehole location and interpolated P- (blue line) and S- (red line) velocities.

¹ Some noise modeling considering P- and S- waves gradient velocity functions down to the sediments-to-bedrock interface have also been performed. These noise simulations are not discussed in the present report.

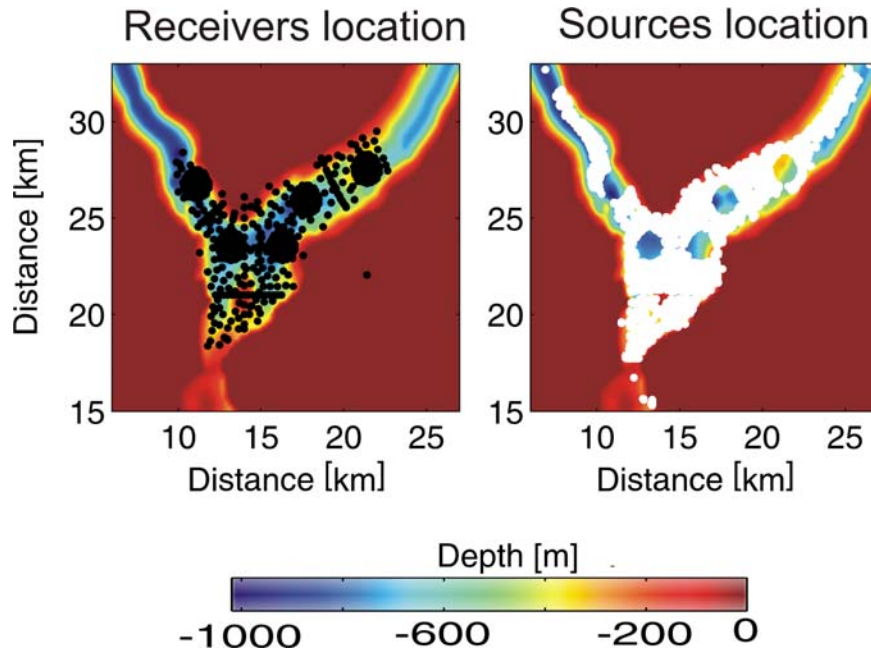


Figure 12: Topography of the low-velocity layer, receivers (black dots) and sources (white dots) location

Table 4: Geophysical parameters for the Grenoble basin

	Vp [m/s]	Vs [m/s]	Qp	Qs	ρ [kg/m ³]
sediments	$19z^{1/2} + 300$ $z < 800$ m 870 $z > 800$ m	$1.2z^{(*)} + 1450$ $z < 800$ m 2410 $z > 800$ m	40	20	$0.4z^{(*)} + 1600$ $z < 800$ m 1920 $z > 800$ m
bedrock	5600	3200	550	360	2500

(*) z is depth in meters

Commentaire : dddd

Table 5: Simulation parameters for the Grenoble basin

Freq. Range [Hz]	Finer grid				Coarser grid				dt
	Grid spacing [m]	X [m]	Y [m]	Z [m]	Grid spacing [m]	X [m]	Y [m]	Z [m]	
0.2 – 1.1	50	33300	33300	1550	150	33300	33300	35400	0.0038

Table 6: List of computations for the Grenoble basin

Dataset #	Duration [s]	Number of sources	Comments
2001	277	30988	Sources located at the surface within the sediment fill
2002	357	5058	Sources located at the surface within the sediment fill

5 Geophysical model of the Basel area

The description of the Basel model given here is mainly based on the work by Kind (2002) and Kind et al. (2003).

5.1 Geophysical parameters

Geometry of the model

At the Geological-Palaeontological Institute of the University of Basel the geologic information for the 3D geologic structure in the area of Basel has been compiled and integrated into a digital model (Zechner et al., 2001). This model presents the geometrical base for the geophysical model. The 3D model consists of seven geological discontinuities and the surface planes of 22 known major faults in the area. An illustrative snapshot of the model is given in Figure 13. The geologic cross section in Figure 17 (lower) is derived from the model and illustrates the six sedimentary bodies enclosed by the geologic interfaces: They are the Quaternary sediments (QUA), the Tüllinger Layers (TUE), the Molasse Alsacienne (ALS), the Meletta layers (MEL), the lower Tertiary and upper Mesozoic sediments (UPM) and finally the Mesozoic sediments (MES). Below the last discontinuity the Paleozoic sediments and crystalline basement rocks (PCB) complete the model. Table 7 lists the stratigraphic units and their abbreviations.

The decision to differentiate and model the interface geometry between the first four geologic units of the model (QUA,TUE,ALS,MEL) was based mainly on the distinct lithology at the bottom of the Quaternary sediments, as it is mapped from the database of boreholes in the Basel area (Noack, 1993). The Tertiary interface below the Meletta layers was modeled because literature values indicated a significant S-wave velocity contrast at this interface. The Mesozoic sediments are included because they form the pre-Quaternary basement rock of the Tabular Jura part of the model. The model covers an area of approximately 400 km² and contains the complete Basel region. In the deepest part of the model in the Rhine Graben the MES/PCB discontinuity reaches a depth of 2000 m.

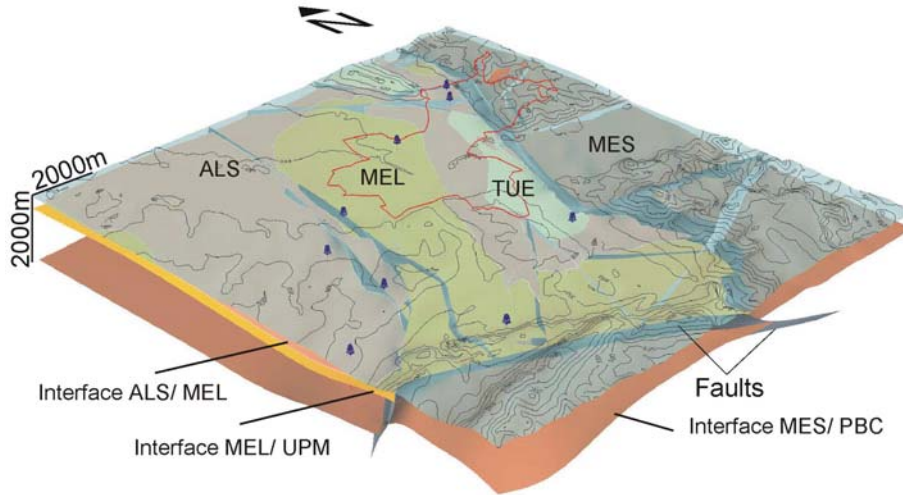


Figure 13: Geologic 3D model geometry (Zechner et al., 2001). Through the transparent topography with contours the geologic units below the surficial Quaternary sediments can be seen (labels as defined in Table 7). Between the red bottom layer and the topography the seismic contrast layer is visible in yellow. The faults included in the model are partially visible as blue shade. Blue drilling rig symbols indicate deep boreholes from which information was available. A red line indicates the limits of the Canton of Basel for orientation.

Table 7: Stratigraphic units represented in the 3D-model and their abbreviations.

Abbreviation	Stratigraphy
QUA	Quaternary sediments
TUE	Tüllinger layers (Tertiary); marls and argillaceous marls
ALS	Molasse Alsacienne (Tertiary); sandy marls
MEL	Meletta layers (Tertiary); sandy and argillaceous marls
UPM	lower Tertiary/ first Mesozoic sediments; Sannoisien (Tertiary) and upper Mesozoic sediments down to Lias
MES	lower Mesozoic; Mesozoic sediments of the Lias and older
PCB	lowest Mesozoic sediments ("Buntsandstein"), Paleozoic sediments ("Rotliegendes") and crystalline basement.

The surface interface is derived from the digital elevation model of the region and therefore quite precise. The second layer representing the pre-quaternary interface is very well constrained from a large database of boreholes down to the Tertiary sediments (Noack, 1993). The uncertainty increases as the density of the borehole data thins out with distance from the inhabited areas. The pre-quaternary surface of the TUE, ALS and MEL derive also from the borehole information. The deeper interfaces are compiled from structural interpretations by

Gürler et al. (1987) and Bitterli et al. (1988). They provide some profile sections and interpreted maps of the MEL/UPM and the MES/PCB discontinuities, based on unpublished seismic cross section data for exploration of natural resources (oil/gas). The information was digitized and then interpolated for the different interfaces with the GOCAD geological object design code (GO-CAD, 1999). In addition, the surfaces of the 22 major known faults in the area were constructed, and intersected according to their likely structural-geological relationship. The final model parts, or volumes, are bound by model horizons representing stratigraphic contacts and modeled fault surfaces. From this approach, the geometry of the geological interfaces is mainly determined through interpolation between the deep boreholes, qualitative constraints and interpretations. An exception is the thickness of the Quaternary sediments, which is well constrained. The geological information on the deeper structures are few, resulting in an uncertainty on the actual position of the interfaces, that increases with depth and lateral distance from the deep boreholes (see Figure 13, drill rig symbols).

Geophysical parameters

The geophysical parameters needed for numerical simulation of seismic wave propagation are density, P-wave velocity, S-wave velocity and the corresponding Q values to model anelasticity. Two studies compiled literature values for the region (Fäh et al., 1997; Steimen et al., 2003). The parameter the least constrained by the literature is the S-wave velocity. This gap was filled by the study of Kind (2002) and Kind et al (2003, 2004). He concentrated his efforts on determining reliable S-wave parameters. P-wave velocities are more readily available and could be taken from two seismic lines. For the deeper lower Tertiary/ first Mesozoic layers sonic-log information from a recent deep borehole (GPI, Basel, 2001) was accessible.

To derive the S-wave velocities for the different layers, the application of an array technique to ambient vibrations was developed by Kind (2002) and Kind et al. (2004). A campaign of five array measurements was performed in Basel (Figure 14, hexagons). The sites were selected to sample the four Tertiary layers in the Rhine-Graben and the upper Mesozoic, where the layer is close to the surface in the Tabular Jura. The measurements constrained the S-wave velocity of the Quaternary and the Tertiary sediments. For the three Tertiary units TUE, ALS and MEL a slight gradient was derived.

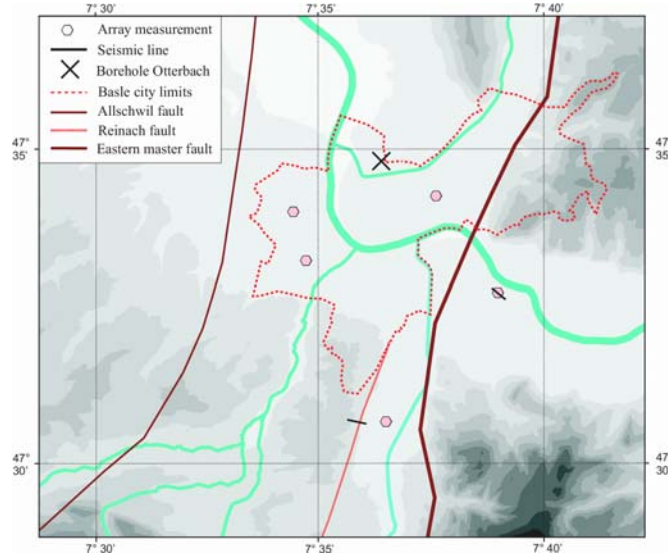


Figure 14 : Overview of the data sources for seismic velocities available for the model (Kind, 2002).

Table 8: Geophysical parameters of the 3D model (Kind, 2002; Kind et al., 2003, 2004). The stratigraphic meanings of the model unit abbreviations are explained in Table 7. The velocity values are averages for the whole layer, the values in parenthesis are minimal and maximal values as either determined in the measurements or in the variability of literature values.

model unit	ρ [kg/m^3]	V_P [m/s]	Q_P	V_S [m/s]	Q_S
QUA	1850	800 ^C (600-1000)	30	450 ^A (400-500)	15
TUE	1850	2200 ^C (1800-2600)	50	725 ^A (650-900)	25
ALS	1850	2200 ^D (2000-2800)	50	650 ^A (600-800)	25
MEL	2000	1800 ^D (1400-2500)	50	600 ^A (450-700)	25
UPM	2350	3400 ^B (3200-3600)	125	2000 ^B (1800-2200)	50
MES	2550	4000 ^B (3600-4500)	125	2350 ^B (2150-2650)	50

^AArray measurement; ^BBorehole sonic log; ^CReflection seismics; ^DLiterature

A deep borehole recently drilled for a geothermal test and exploration was accessible and provided caliber, gamma-ray/density and sonic logs (GPI Basel, 2001). The position of the borehole is marked as cross in Figure 14. For the softer sediments above the lower Tertiary/first Mesozoic no data was available due to technical difficulties in the borehole. The velocity values are practically constant, with variations corresponding to caliber variations in the borehole.

P-wave velocity data from two seismic profiles were accessible from sites indicated as lines in Figure 14. One reflection seismic line was done in a paleoseismic study across the Rheinach fault causing the 1356 earthquake (Meghraoui et al. 2001), the other line is unpublished so far (F. Nitsche, personal communication). The interval velocities derived for the time to depth conversion in the seismic profiles were used for the P-wave velocities in the Quaternary and Tüllinger layers and they also confirmed the P-wave velocities in the lower Mesozoic. Finally the P-wave velocities for the Molasse Alsacienne and the Meletta layers had to be taken from the literature (Clark (Ed.), 1966). The densities and Q values derive from literature values and estimates collected in the earlier studies (Fäh et al. , 1997; Steimen et al., 2003).

The collection of all average values and the uncertainty ranges in the velocities are listed in Table 8. For the Tertiary layers TUE, ALS and MEL a velocity gradient is used to refine the model.

Refinement of the model geometry with H/V polarization

At this stage the model consists of the collection of all necessary information and its uncertainty. To verify and refine the model, Kind (2002) and Kind et al. (2003) used the data from a H/V polarization survey that provided fundamental frequencies for the Basel area. The fundamental frequency can be calculated in a simple way from the geophysical model and therefore provides a simple means for validation of the model. Because of the irregular distribution of the H/V polarization measurement points and the focus of the interest on the city of Basel, the validation was limited to the area of the city of Basel itself. Over the Tabular Jura no attempt at model validation was done: The shorter wavelength associated with the higher fundamental frequencies are more sensitive to lateral inhomogeneities, so variations in the composition of the soft sediments are of higher importance.

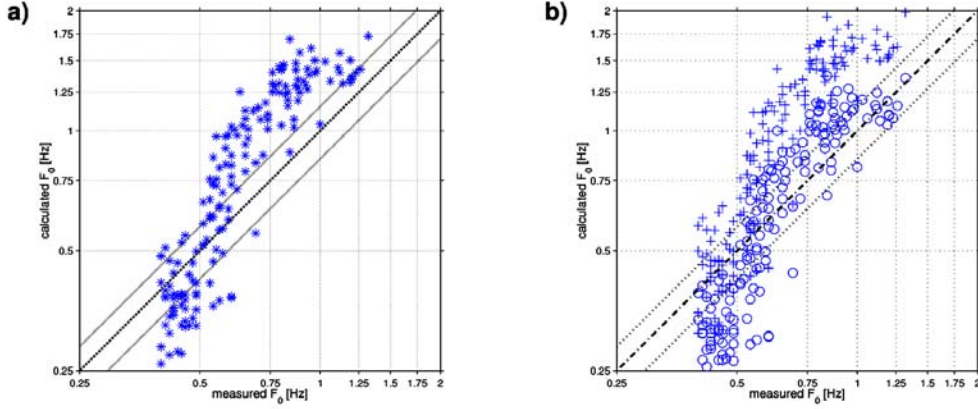


Figure 15: Measured versus calculated fundamental frequencies from the model before the corrections to the geology. The dotted range marks the uncertainty margin in the measured frequencies. Part a) shows the values calculated with the average S-wave velocity model, while part b) shows the values calculated with the maximum S-wave velocities as crosses and circles for the minimal S-wave velocity models (from Kind, 2002).

For all measurement sites within the Rhine Graben and inside or close to the border of Basel (160 out of 250), a 1D sediment profile was extracted from the digital 3D model. The relevant contrast for the H/V polarization is between the Meletta layers and the lower Tertiary/first Mesozoic, clearly identified from the velocity model. Fundamental frequencies were then calculated as vertical 4-way S-wave travel times between surface and the contrasting interface. Figure 15a) shows the comparison of calculated and measured frequencies before the correction to the geometry of the 3D model. The dotted lines indicate the uncertainty margin in the measured frequencies. The maximal and minimal S-wave velocities derived for the geophysical model were used to calculate upper and lower limits as well. The corresponding values are shown in Figure 15b) as crosses for the maximum and circles for the minimum velocity model. In the higher frequency range, the calculated frequencies are too large. Even considering the uncertainties in the S-wave velocity and the measurements does not give an acceptable agreement. The concerned sediment depth ranges between 50 m and 100 m from the surface, where the S-wave velocity is very well constrained through the array measurements, so the velocity model cannot be the cause for the discrepancy.

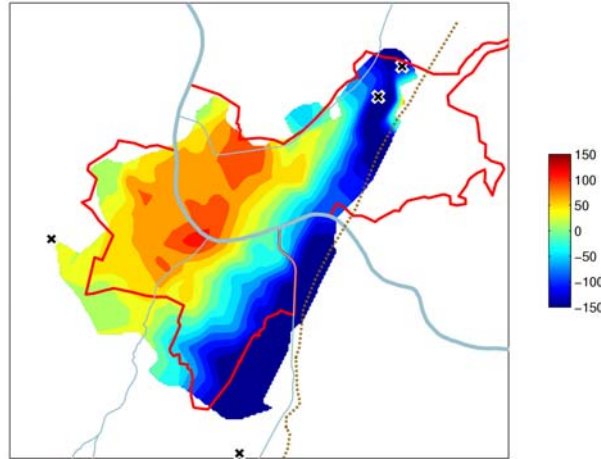


Figure 16: Magnitude of the corrections applied to the model geometry at the bottom of the Meletta layer in meters. Positive values indicate an increase of the thickness, negative values a decrease. Crosses mark the location of deep boreholes constraining the deeper interfaces (from Kind, 2002).

The fundamental frequency measurements are well constrained as well, considering their stability and conservative uncertainty constraint of 15%. This suggests that the error lies in an underestimation of the thickness of the sedimentary layers in this part of the model, which is based on extrapolation from data points at distances in the order of kilometers. Comparison of the S-wave measurement inversion with the digital model had already indicated the same, but the most convincing piece of evidence are the results from the newly accessible data of the deep borehole Otterbach (GPI Basel, 2001), which confirmed the corrections on the horst of Basel.

The much lower calculated values for the measured frequencies below 0.6 Hz cannot be explained by the uncertainty in the constant velocity model either. The gradient visible in the array measurements can reduce the difference slightly, but it cannot explain the difference fully either. Estimated theoretical 2D resonance frequencies determined for a section of the syncline of St. Jacob Tüllingen by Steimen (1999) coincide with the theoretical 1D fundamental frequencies and the H/V peaks as well. So it is possible, that the low in the syncline is associated with a 2D resonance, but so far no conclusive data is available for discriminating the 1D and the 2D case in Basel. Weighting the lack of hard data on the geometry of the model at depth against the uncertainty of the velocity model in the deeper sediments and the 2D/1D question, Kind (2002) favored a correction of the geometry to the 1D interpretation in order to

get a model from a consistent approach. The amplification calculations justified the approach, as the amplification peaks coincide with the fundamental frequencies. But the spatial extent of the amplification peaks is so widespread across the syncline, such that a 2D interpretation can neither be identified nor ruled out.

From the deviations at all measurement point corrections to the depth of the MEL/UPM interface were calculated and integrated in the model (Kind, 2002). The magnitude of the corrections is shown in Figure 16, they range from more than 50 m over the horst of Basel to more than 100m within the Rhine Graben. In the construction of the geological model, the interfaces in the Tertiary layers depend on each other. So the modification of the MEL/UPM interface initiates corrections to the ALS and TUE layers as well. The effects are illustrated in Figure 17, where sections along identical coordinates are shown for the initial and the corrected model. The modifications from the fundamental frequencies concern the dominant seismic contrast (black line) in the model. The layers MEL, ALS and TUE are then constructed with thickness constraints and information from the geology below the Quaternary surface sediments. Over the horst of Basel only the MEL layers are concerned, their depth is significantly increased below the city. In the syncline of St. Jacob Tülingen the modifications are most significant, here all three sedimentary layers are reduced in thickness. Within the fault zone of the Rhine Graben master-fault the model is modified as well, but the geometry of interfaces is unknown, because of probable staggering of the fault and deformations of the layering. As the approximation of horizontal layering breaks down in the fault zone, fundamental frequencies cannot be interpreted in this zone. Figure 18 shows the comparison results from the model with the newly interpolated lower Meletta interface proposed by Kind (2002). A very interesting result is that the uncertainty of approximately 15% in the determination of the fundamental frequency from measurements matches the uncertainty in the resulting frequency from the possible ranges in the S-wave velocity model.

With the corrections on the 3D model a consistent geophysical 3D model could be derived by Kind (2002). All available geological information has been integrated and led to the 3D geometry of the model. For the geophysical parameters of the model also all available information has been considered and the largest gap, the S-wave velocities, was filled with measurements.

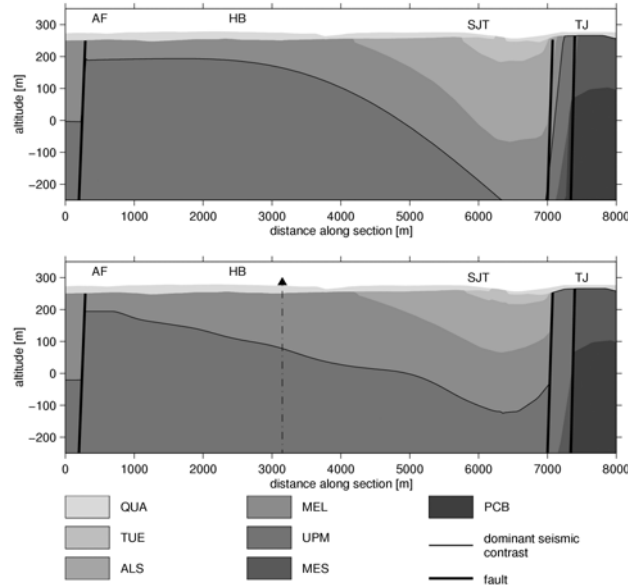


Figure 17: Illustration of the corrections to the geologic model proposed by Kind (2002). The upper part of the figure shows a section from the initial model, while the lower part of the figure shows the same section after the correction. The labeled structures are the Allschwil fault zone (AF), the horst of Basel (HB), the syncline of St. Jacob Tüllingen and the Tabular Jura (TJ). A triangle and a dash dotted line indicate the area of the horst of Basel where the new borehole confirmed the corrections to the model geometry.

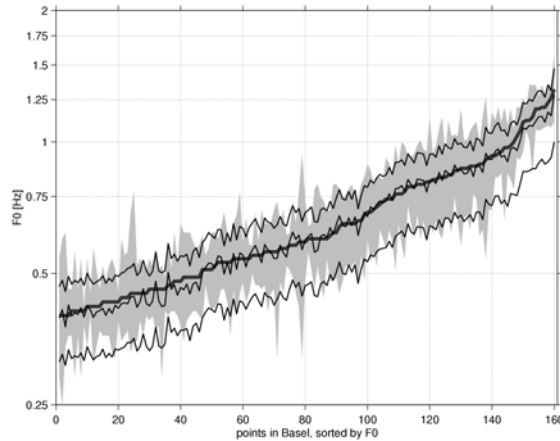


Figure 18: Measured versus calculated fundamental frequencies from the corrected geometrical model. The measured f_0 (thick gray line) is shown sorted by value with the gray shaded area indicating the uncertainty from the interpretation of the H/V ratios. The thin black lines show the calculated f_0 and the uncertainty range in the calculations derived from the uncertainty in the S-wave velocity model (Kind, 2002).

5.2 H/V and array experiment

Several aforementioned array and H/V measurements have been performed by Kind (2002) and are indicated in Figure 19. The H/V data were collected in 1995, 1999 and 2000, totalling 309 measured sites. Duration of measurements was about 15 minutes at each site and sensors (Lennartz Le3D-5s) were placed either on soil either on the asphalt of the sidewalk. Five array measurements have been performed using 1s sensors connected to Mars88 instruments and measurements lasted 6 minutes. The precision of the DCF77 timing synchronization of the instruments was tested to be 1 ms (Kind, 2002). Within the SESAME project, three other array measurements have been performed in April 2002 nearby the Swiss-German border (Figure 20). All the information regarding these last measurements may be found in the SESAME Deliverable D06.05 “Array data set for different sites”.

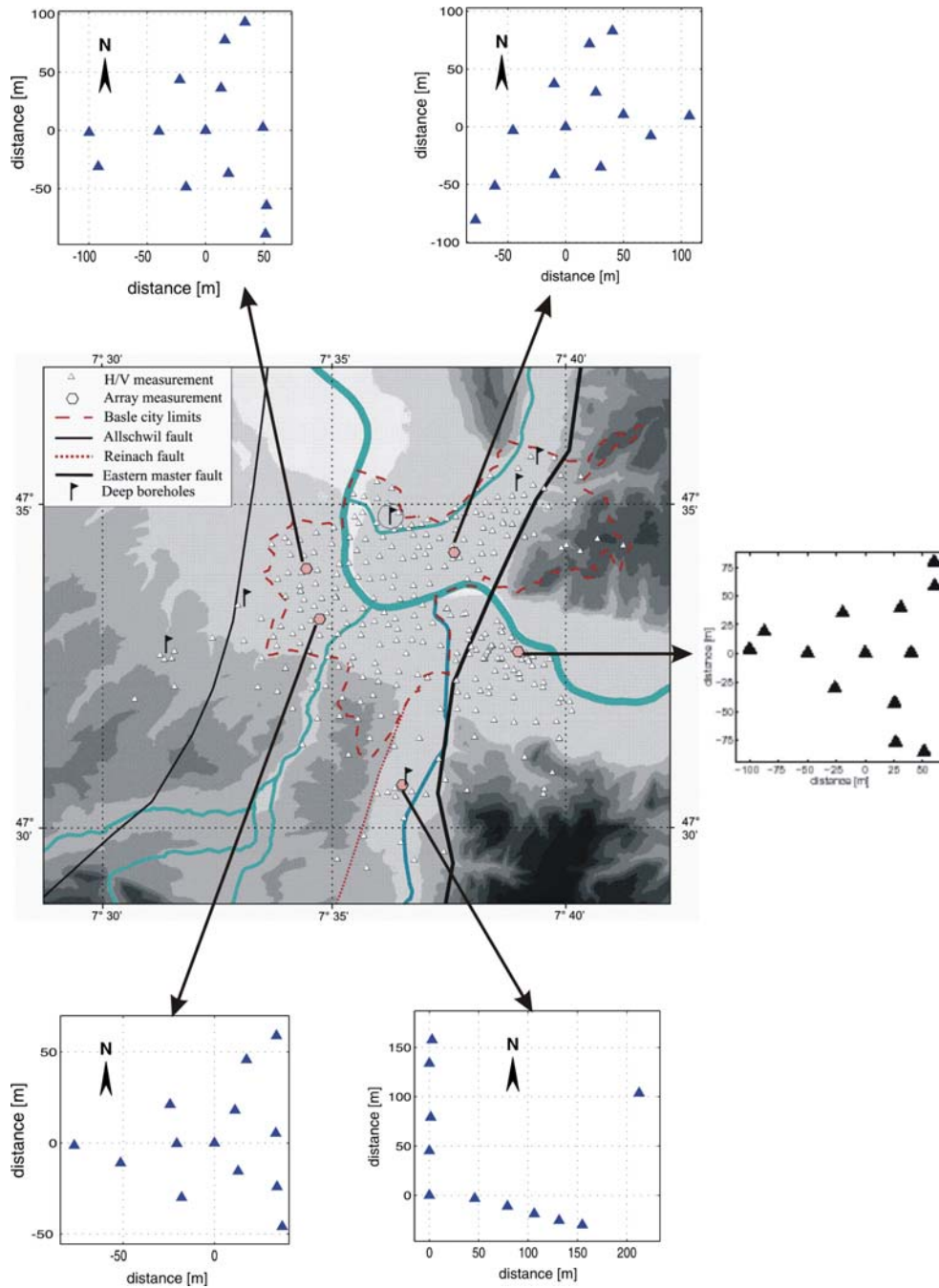


Figure 19: H/V (triangles) and array (filled circles) measurements within the Basel area (after Kind, 2002). The topography is indicated in gray scale.

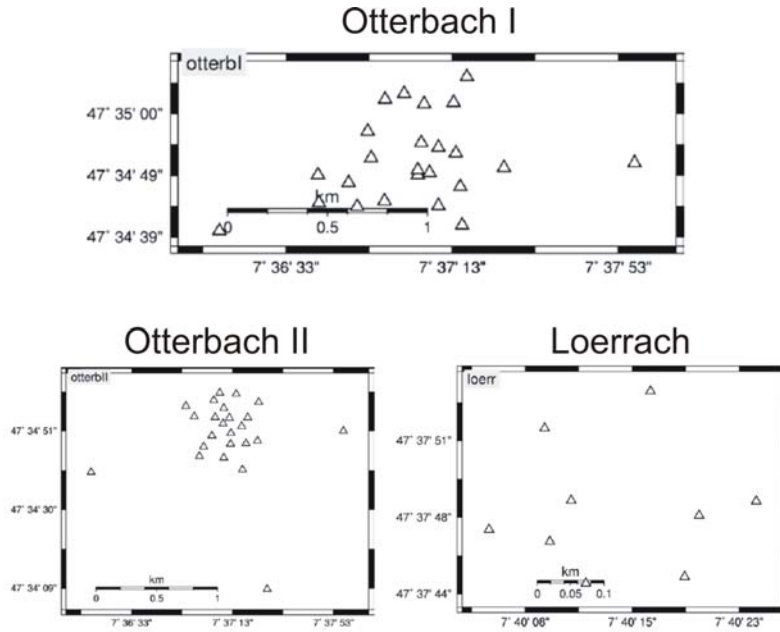


Figure 20: Array geometries at the three measured sites within the SESAME project (SESAME Deliverable D06.05)

5.3 Noise simulation

Since the noise modelling is appropriate for models having a flat free surface, we did not consider the topography above the average altitude (250 meters) of the Basel city. We have introduced 3396 receivers located at the surface (Figure 21), some of them fitting the real noise measurements (H/V and array). Sources are composed of 50% of delta-like and 50% of pseudo-monochromatic signals that have been randomly distributed at the free surface within the basin (Figure 21). The geophysical parameters of the different layers introduced in the noise modeling are indicated in Table 9, and the layers topography is displayed in Figure 22. The parameters used for the FD simulation (grid spacing, frequency bands, size of the finer and coarser FD grids) are indicated in Table 10. At the present writing time, the first computation for this model is still running (Table 11).

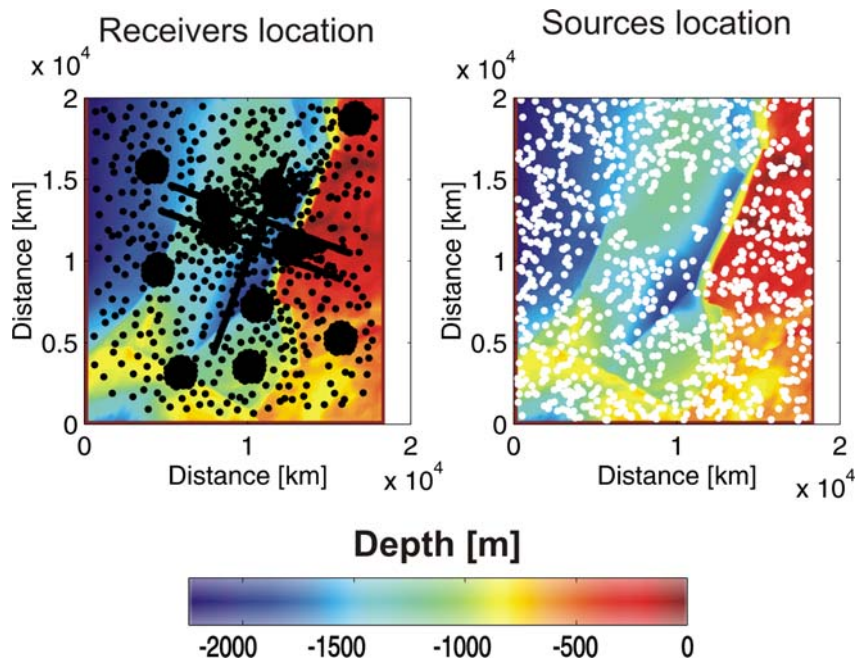


Figure 21: Topography of the bedrock, receivers (black dots) and sources (white dots) location

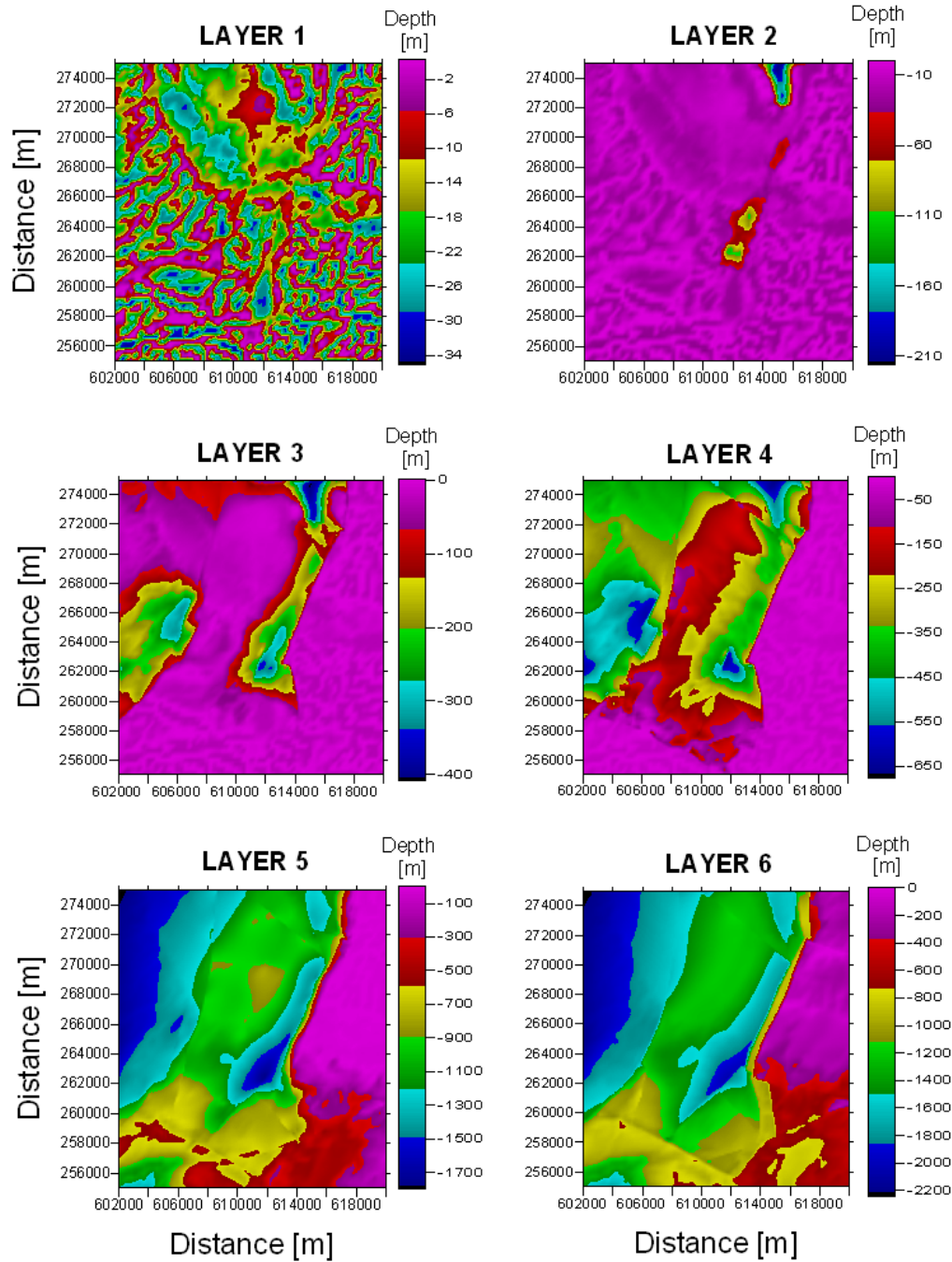


Figure 22: Topography of the layers given in Table 9. Distances are given in the Swiss coordinates system.

Table 9: Geophysical parameters for the Basel basin. The layer name specifies the geological unit below the interface, valid to the next interface. The parameters are then given as a function of depth. The Z value indicates the depth from the surface for which the parameters are valid.

	Z [M]	VP [M/S]	VS [M/S]	QP	QS	ρ [KG/M3]
Layer 1	> 0	900	450	30	15	1850
Layer 2	25	2000	650	50	25	1850
	50	1800	650	50	25	2000
	75	1800	850	50	25	2000
	100	1800	925	50	25	2000
	150	1800	1000	50	25	2000
	200	1800	1025	50	25	2000
	250	1800	1050	50	25	2000
	300	1800	1075	50	25	2000
	350	1800	1100	50	25	2000
	400	1800	1125	50	25	2000
	450	1800	1150	50	25	2000
	500	1800	1175	50	25	2000
	550	1800	1200	50	25	2000
	> 550	1800	1225	50	25	2000
Layer 3	25	1900	575	50	25	1850
	50	1800	575	50	25	2000
	75	1800	675	50	25	2000
	100	1800	725	50	25	2000
	150	1800	775	50	25	2000
	200	1800	825	50	25	2000
	250	1800	850	50	25	2000
	300	1800	875	50	25	2000
	350	1800	900	50	25	2000
	400	1800	925	50	25	2000
	450	1800	950	50	25	2000
	500	1800	975	50	25	2000
	550	1800	1000	50	25	2000
	> 550	1800	1025	50	25	2000
Layer 4	25	1800	500	50	25	2000
	50	1800	600	50	25	2000
	75	1800	600	50	25	2000
	100	1800	600	50	25	2000
	150	1800	650	50	25	2000
	200	1800	650	50	25	2000
	250	1800	700	50	25	2000
	300	1800	700	50	25	2000
	350	1800	750	50	25	2000
	400	1800	750	50	25	2000
	450	1800	800	50	25	2000
	500	1800	800	50	25	2000
	550	1800	850	50	25	2000
	> 550	1800	850	50	25	2000
Layer 5	>0	3400	2000	125	50	2500
Layer 6	>0	4200	2400	125	50	2550
Bedrock	>0	5200	2800	125	50	2650

Table 10 : Simulation parameters for the Basel modeling

Freq. Range [Hz]	Finer grid				Coarser grid				dt
	Grid spacing [m]	X [m]	Y [m]	Z [m]	Grid spacing [m]	X [m]	Y [m]	Z [m]	
0.3 – 2.2	35	20370	18375	2450	105	20370	18375	25410	0.0030

Table 11 : List of computation for the Basel model

dataset #	Duration [s]	Number of sources	Comments
1001	> 325 s	?	Sources located at the surface within the sediment fill

6 Comparison between real and synthetics noise data: example of Grenoble and Colfiorito basins

In the following, we present comparison between simulated and the real noise data at the array sites for Grenoble and Colfiorito. For this study, we have used the data set #1003 and #1004 (Table 2) for the Colfiorito site and the first 4 minutes of the data set #2002 for the Grenoble basin (Table 6).

6.1 H/V, array analysis and inverted seismic profiles

The H/V ratios were computed using the procedure developed within the SESAME project (SESAME Deliverable D08.02) and the same processing parameters were used for both simulated and observed data. The frequency-wavenumber based methods ($f-k$) are often used for deriving the phase velocity dispersion curves from ambient vibration array measurements. In this study, we have used the conventional semblance-based frequency-wavenumber method (CVFK) and/or the High-Resolution frequency-wavenumber method (CAPON) implemented in the CAP software developed within the SESAME project (SESAME Deliverable D18.06; Ohrnberger et al., 2004a, 2004b). Operating with sliding time windows in narrow frequency bands, these methods provide the wave propagation parameters (azimuth and slowness as a function of frequency) of the most coherent plane wave arrivals. The inverted seismic profiles were then obtained using an Neighbourhood algorithm developed within the SESAME project by Wathelet et al. (2004).

6.2 H/V and array techniques on simulated noise

H/V technique

We have compared the H/V peak frequencies computed on the simulated noise with the theoretical 1D resonance frequencies given by the 1D transfer function for vertically incident S-waves. When comparing frequencies, no standard deviation for the peak frequency estimates was considered since the short duration of the noise time series did not allow meaningful statistics. Figure 23 and Figure 24 display for both sites: (a) a contouring display of the 1D resonance frequency estimated at each receiver location, (b) a contouring display of the H/V peak frequency, (c) the relative deviation (in %) of the H/V peak frequencies from the 1D resonance frequencies, (d) the H/V peak frequency as a function of the 1D resonance frequency. For Colfiorito basin (Figure 23), the H/V peak frequencies map very well the low-velocity layer thickness variation throughout the basin. Moreover, most of the H/V peak frequencies agree within a deviation range of 10-20% with the 1D frequencies, the most extreme deviation are found for receivers that are located at the border of the model or above local topographical troughs. For Grenoble basin (Figure 24), the H/V peak frequencies are correlated with the thickness variation. However, most of the H/V peak frequencies significantly overestimate the theoretical 1D local frequency, within a relative deviation up to 50%. This overestimation most probably come from the fact that, even though both Colfiorito and Grenoble basin exhibit 3D geometries, the width-to-thickness ratio of the structure is much smaller for Grenoble than for Colfiorito, which should lead the structure having resonance frequencies (2D/3D eigenvibrations) significantly differing from the 1D local resonance frequencies (Bard and Bouchon, 1985; Roten et al., 2004).

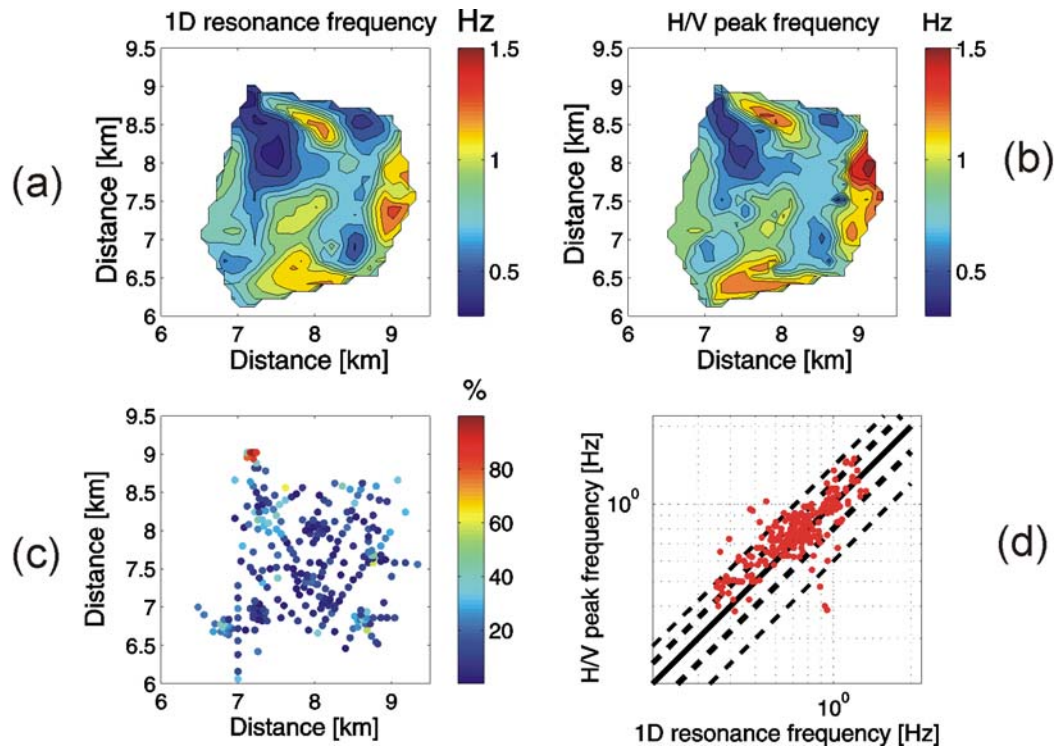


Figure 23: Noise simulation for Colfiorito basin: (a) contouring display of the 1D resonance frequencies estimated at each receiver location; (b) contouring display of the H/V peak frequency; (c) relative deviation of the H/V peak frequencies from the 1D resonance frequencies; (d) H/V peak frequency as a function of the 1D resonance frequency, the 1:1 relative deviation from the 1D resonance frequency is indicated by the thick black line, the 20% and 40% deviation are indicated by the thick and thin dashed lines, respectively.

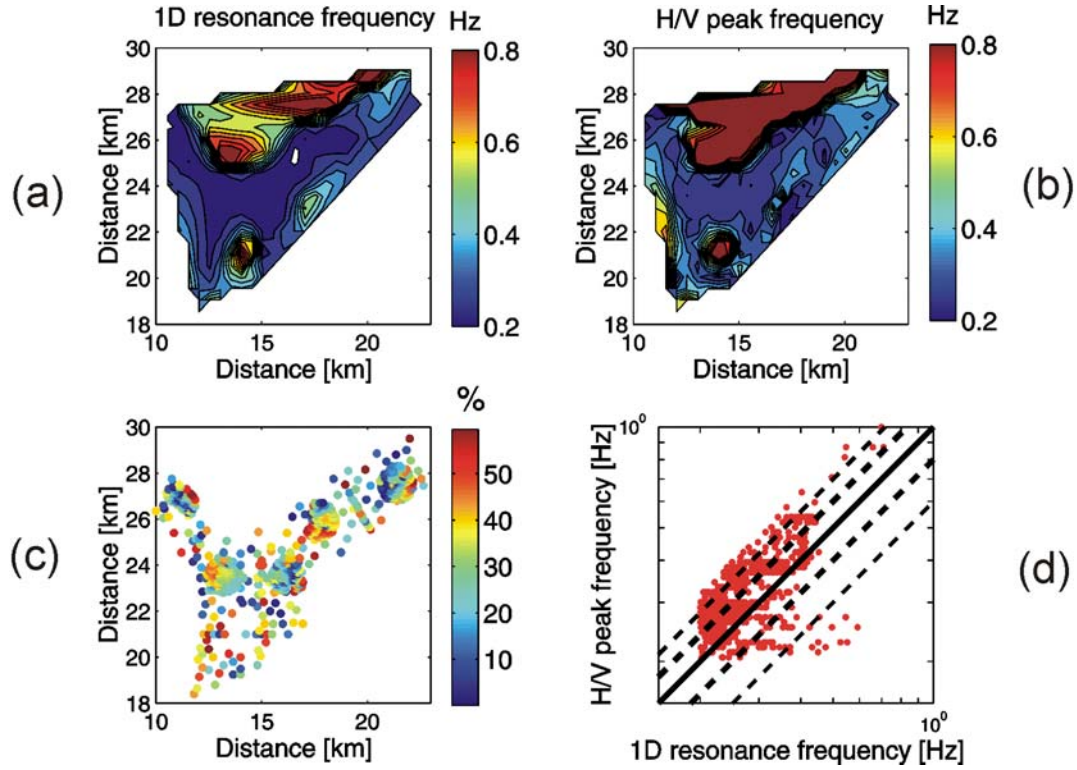


Figure 24: Noise simulation for Grenoble basin: (a) contouring display of the 1D resonance frequencies estimated at each receiver location; (b) contouring display of the H/V peak frequency; (c) relative deviation of the H/V peak frequencies from the 1D resonance frequencies; (d) H/V peak frequency as a function of the 1D resonance frequency, the 1:1 relative deviation from the 1D resonance frequency is indicated by the thick black line, the 20% and 40% deviation are indicated by the thick and thin dashed lines, respectively.

Array technique

For the array analysis, we have used arrays similar in geometry and in location to those that have been deployed in the field. For Colfiorito basin, all arrays have been used. For Grenoble basin, only the largest aperture arrays (arrays F and H in Figure 8 and the large array displayed in Figure 9) were considered since the upper frequency in the noise modeling is 1.1 Hz.

Colfiorito basin

The arrays B and E are located above an almost flat sediment-to-bedrock topography, while arrays A and C are located above local topographical troughs (Figure 3 and Figure 25). For

array C, only the receivers that did not exhibit flat H/V curves (Figure 25, black dots) were considered in the analysis. The array analysis was performed using a wavenumber domain equidistantly sampled in slowness and azimuth (azimuthal and slowness resolution set to 5 degrees and 25 s/m, respectively). The time window length of analysis was fixed to 7 times the central period $1/f_c$ of the analyzed frequency band $[0.9f_c \ 1.1f_c]$. Furthermore, successive time-windows of analysis were overlapped by 50% in all frequency bands. For the inversion, the starting model was a layer over halfspace. At all sites, the inversion has been performed using a band-limited portion of the estimated dispersion curve, from the H/V peak frequency of the site up to 2.7-3 Hz. The array analysis did not indeed provide reliable estimates of the phase velocities at frequencies below the resonance frequency because of the lack of coherent energy. This may be due to the limited aperture of the array or/and the fact that we do not include in the simulation the effects of impinging coastal surface waves that propagate at low frequency throughout the crustal structure.

Figure 26 displays for each array the inverted P- and S- wave velocity profiles as well as the measured phase velocities and Figure 27 shows the measured dispersion curves and the dispersion curves of the fundamental Rayleigh waves mode computed using 1D soil profiles that correspond to the maximum, minimum and average sediment thickness below the array. For arrays B and E, the P- and S- waves velocities are very well estimated within the sediments. The sediment thickness is slightly overestimated by 10 to 20% and the velocities in the bedrock are rather close (within 20%) to the ones introduced in the noise modeling. Besides, the estimated dispersion curves fit well the 1D local dispersion curves (Figure 27), suggesting that the noise wave field at those array sites is dominated by 1D wave propagation. For the arrays A and C below which the sediment thickness is rapidly varying, the P- and S- wave velocities within the sediments are well estimated while the velocities in the bedrock are largely underestimated. The inverted sediment thickness seems to be basically related to the average thickness under the array. It has also to be pointed out that the sediment thickness variation below these array sites results in measured dispersion curves deviating from the 1D dispersion curves (Figure 27).

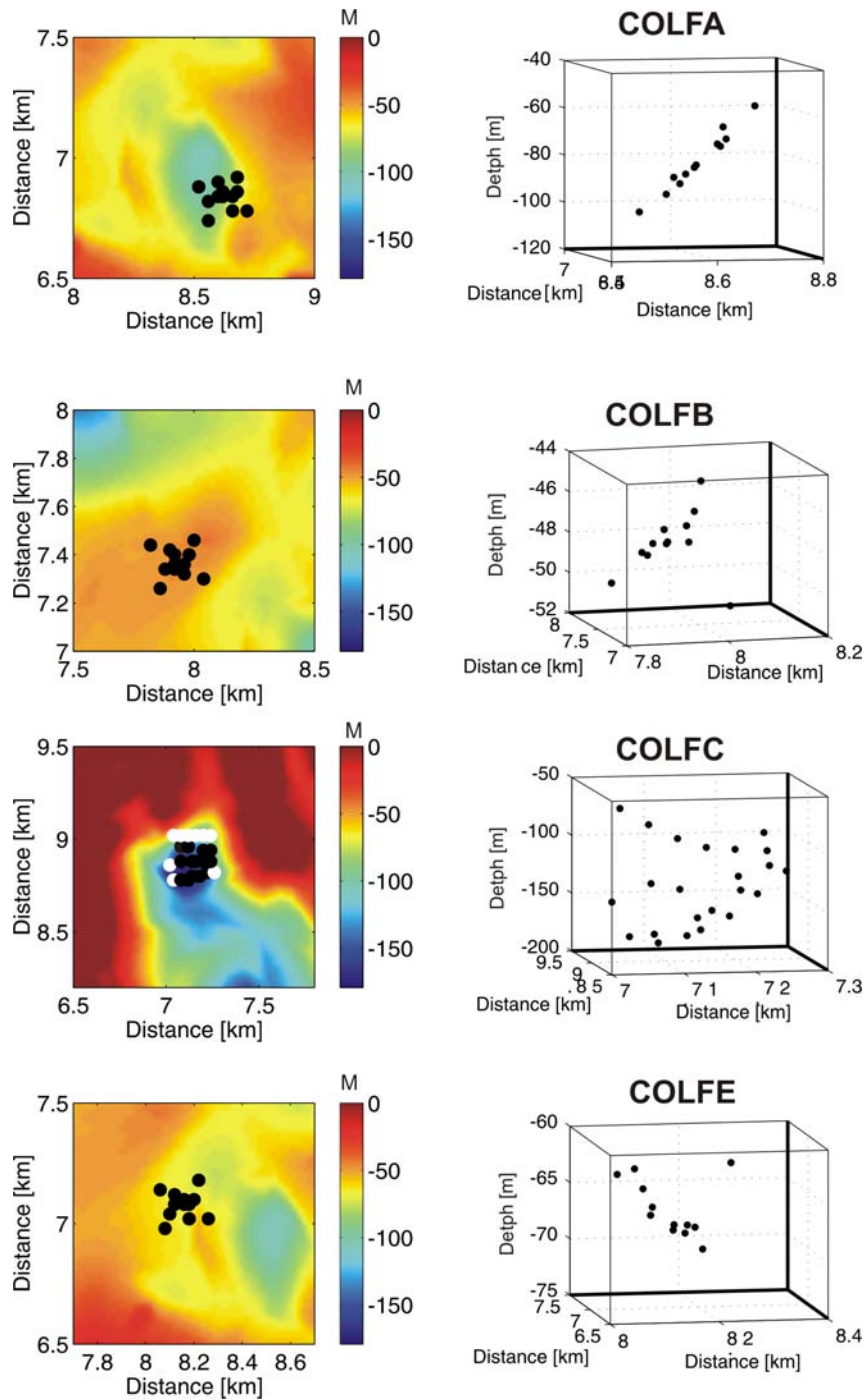


Figure 25: (left) topography of the low-velocity layer and array geometry (black dots); (right) depth of the bedrock below each receiver. The white dots for COLFC array indicate receivers that were not used in the array analysis. See Figure 3 for the arrays location within the basin.

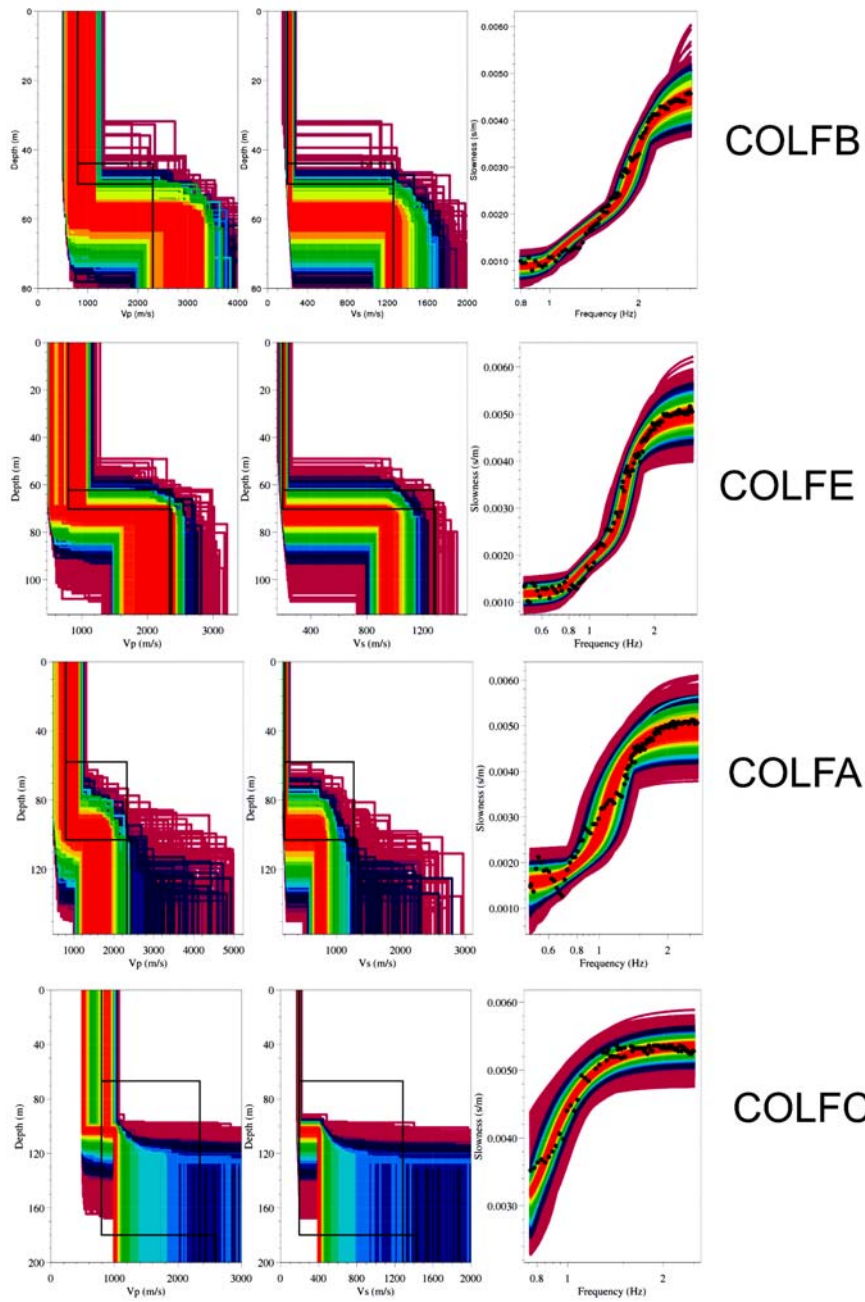


Figure 26: Noise simulation for Colfiorito basin: inverted P- and S- wave velocities and measured dispersion curves (black dots) for Colfiorito basin. The black lines indicate the velocity profiles related to the minimum and the maximum sediment thickness below the array. See Figure 3 for the arrays location within the basin.

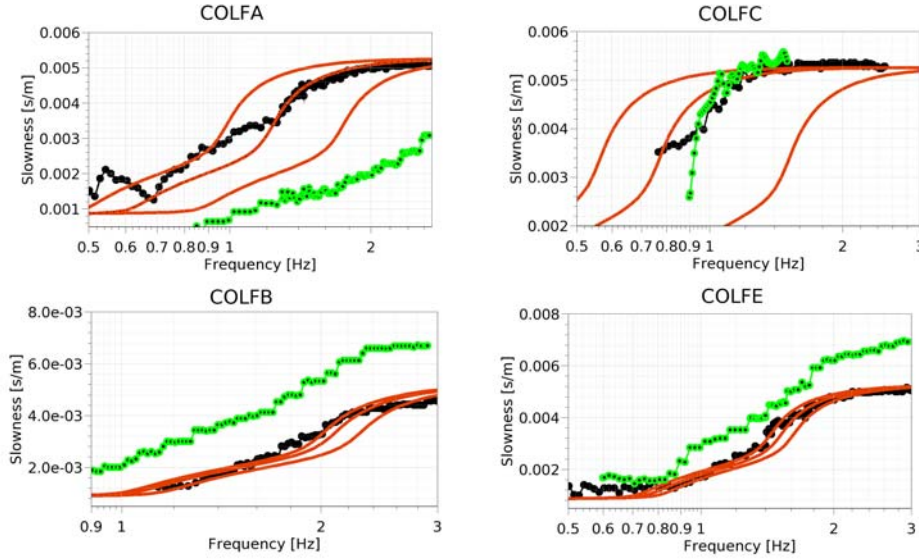


Figure 27: Dispersion curves estimated using simulated noise data (black dots) and real noise data (green dots). The red lines indicate the dispersion curves of the fundamental Rayleigh waves mode computed using 1D soil profiles that correspond to the maximum, minimum and average sediment thickness below the array.

Grenoble basin

In the following, arrays F and H (Figure 8) are called “Synchrotron” and “Campus” and the large array displayed in Figure 9 is called “Bon Pasteur”. The sediment thickness varies significantly below the array sites as displayed in Figure 28. The array analysis was performed using a wavenumber domain equidistantly sampled in slowness and azimuth (azimuthal and slowness resolution set to 5 degrees and 25 s/m, respectively). The time window length of analysis was fixed to 7 times the central period $1/f_c$ of the analyzed frequency band $[0.9f_c \ 1.1f_c]$. Furthermore, successive time-windows of analysis were overlapped by 50% in all frequency bands. For the inversion, the starting model was a power-law gradient layer over halfspace. At all sites, the inversion has been performed from the H/V peak frequency of the site up to 1 Hz. Figure 29 displays the inverted P- and S- wave velocity profiles as well as the measured phase velocities at each array site and Figure 30 shows the measured dispersion curves and the dispersion curves computed using 1D soil profiles that correspond to the maximum, minimum and average sediment thickness below the array. For all arrays, the velocities in the bedrock are poorly constrained, which could be explained by the lack of coherent energy at frequencies below the resonance frequency of the site, as previously mentioned. Down to the estimated

sediments-to-bedrock interface, S-wave velocities are rather well estimated at all the array sites. For Bon Pasteur and Campus sites, the estimated sediment thickness is lower than the minimum sediment thickness below the array, while for Synchrotron site, the estimated sediment thickness ranges in-between the minimum and the maximum sediment thickness observed below the array. Such underestimation of the sediment thickness might come from the frequency band-limited portion of the dispersion curve used in the inversion procedure as it is slightly indicated in Figure 31 that displays the inverted P- and S- wave velocities for a theoretical dispersion curve computed for a 1D soil profile having the same gradient velocities as for the Grenoble model and a sediment thickness of about 630 m. However, keeping in mind that most of the H/V peak frequencies significantly overestimate the theoretical local 1D local frequency, the sediment thickness underestimation would rather be explained by a complex 2D/3D wave field propagation as it is observed in alpine valleys (Cornou et al., 2003, Roten et al., 2004).

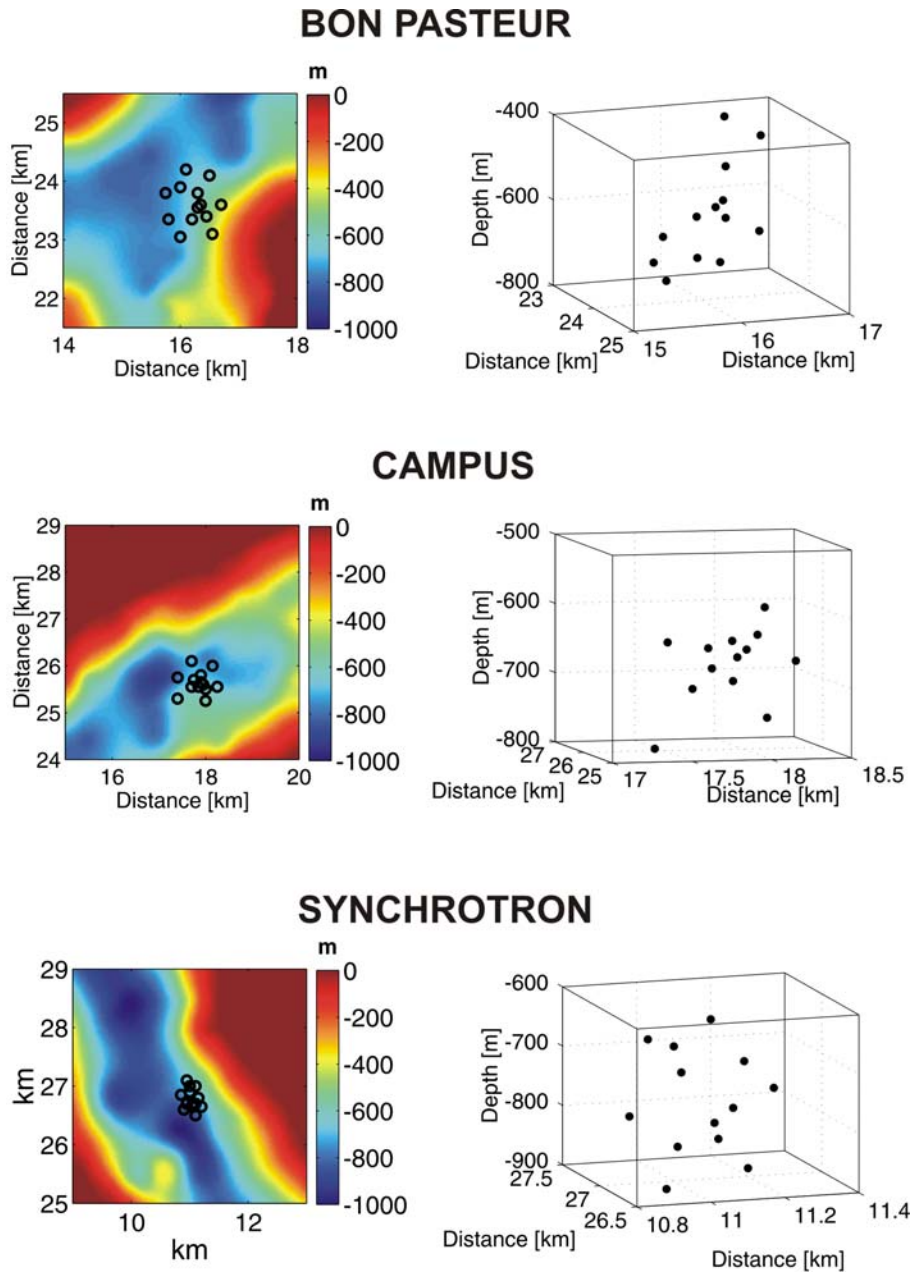


Figure 28: (left) topography of the low-velocity layer and array geometry; (right) depth of the bedrock below each receiver

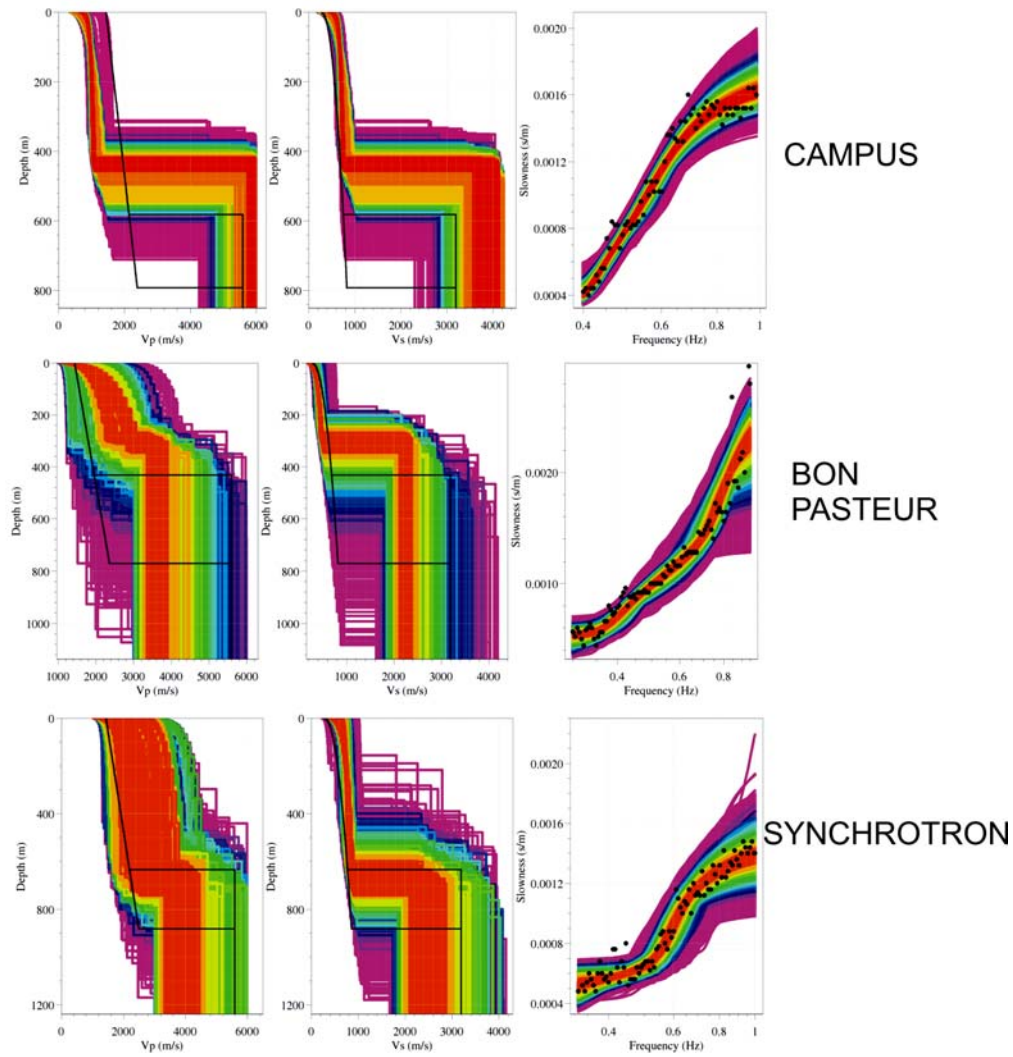


Figure 29: Noise simulation for Grenoble basin: inverted P- and S- wave velocities and measured dispersion curves (black dots) for Grenoble basin. The black lines indicate the velocity profiles related to the minimum and the maximum sediment thickness below the array

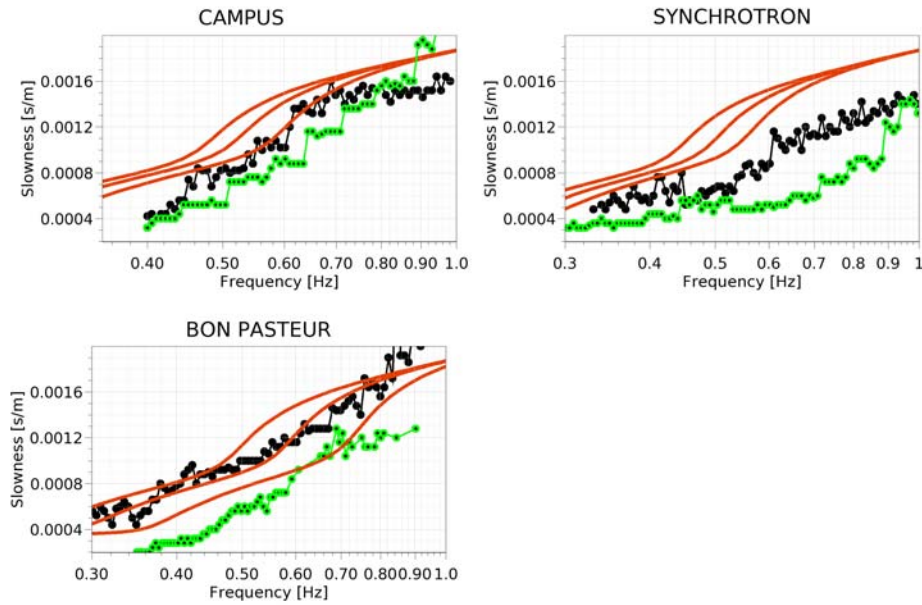


Figure 30: Dispersion curves estimated using simulated noise data (black dots) and real noise data (green dots). The red lines indicate the dispersion curves of the fundamental Rayleigh waves mode computed using 1D soil profiles that corresponds to the maximum, minimum and average sediment thickness below the array.

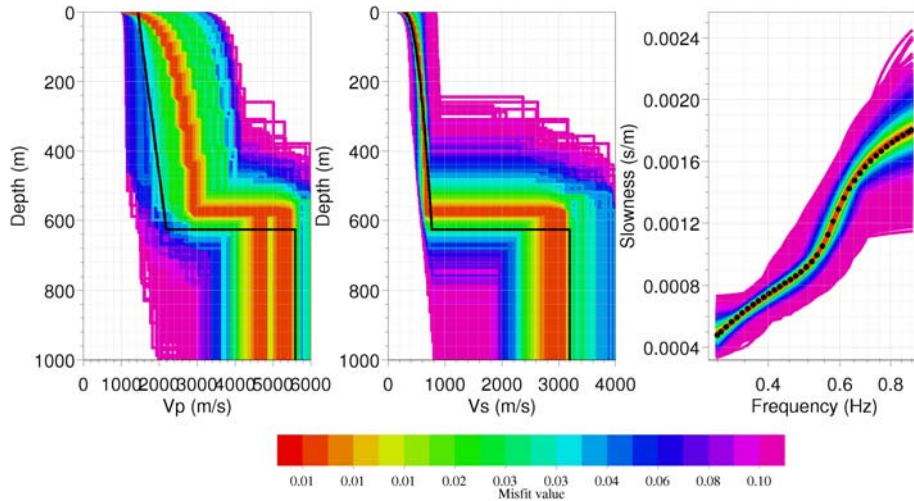


Figure 31: Inverted P- and S- wave velocities for the theoretical dispersion curve of the fundamental Rayleigh waves mode indicated in the right panel (black dots). The black lines indicate the velocity profiles used for the computation of the theoretical dispersion curve.

6.3 Comparison with the actual ambient noise

6.3.1 Colfiorito basin

Figure 32 displays for one representative receiver at each array site the H/V curve computed for both simulated and real data. While simulated and real H/V curves are similar at arrays B and E, they significantly differ at arrays A and C. For the array analysis on real noise data, we have used twenty minutes of ambient noise and used the same processing parameters as for the simulated noise data within the 0.3-3.3 Hz frequency band. The inversion was performed between the H/V peak frequency and around 2.5-3 Hz. The inverted S- wave velocity profiles using simulated and real ambient noise are rather close as indicated in Figure 33. The main difference between real and simulated noise is the estimated S-wave velocity within the surficial layer that is lower than 200 m/s for arrays B and E that exhibit an average velocity of about 170 m/s. For array A, the average velocity is about 300 m/s. These differences in velocities are also clearly seen in Figure 27 and explain, at least for arrays B, E and A, the main differences between H/V and dispersion curves derived from simulated and real noise data. The differences between H/V curves obtained at array C for simulated and real noise data can not be interpreted as resulting of difference in S-wave velocities since the dispersion curves computed for simulated and real noise data are rather close (Figure 27). At this time we do not have consistent arguments to draw clear conclusions about the differences observed in H/V curves using simulated and real noise data. However, especially interesting for array C is the back-azimuth distribution as a function of slowness as depicted in Figure 34: while for arrays A, B and E, the slowness is increasing with frequency as a result of surface wave propagation properties, a back-azimuth at a very small slowness is observed for array C whatever the frequency, which may be related to local 3D resonance effects.

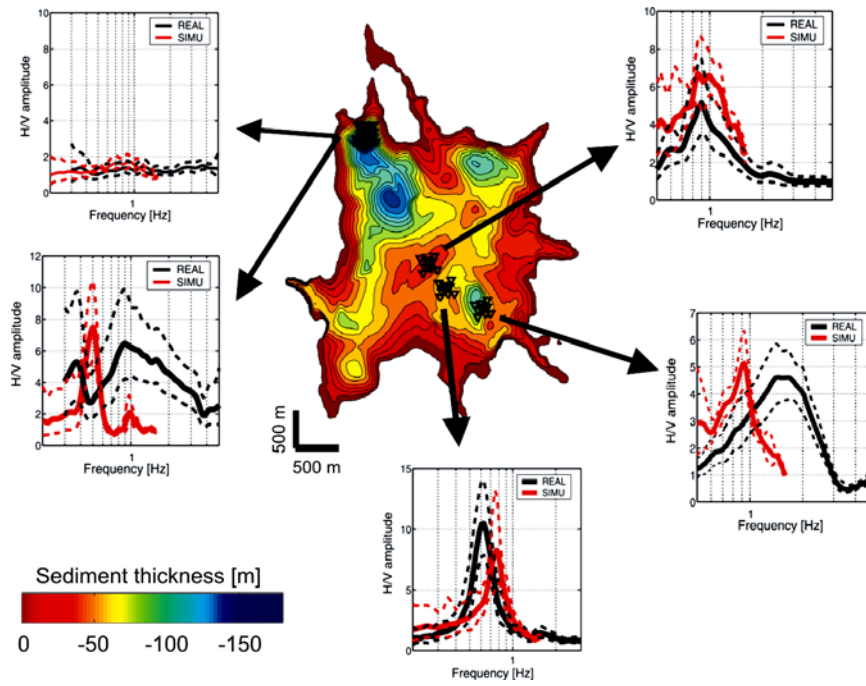


Figure 32: H/V curves computed using simulated (red curves) and real (black curve) noise data

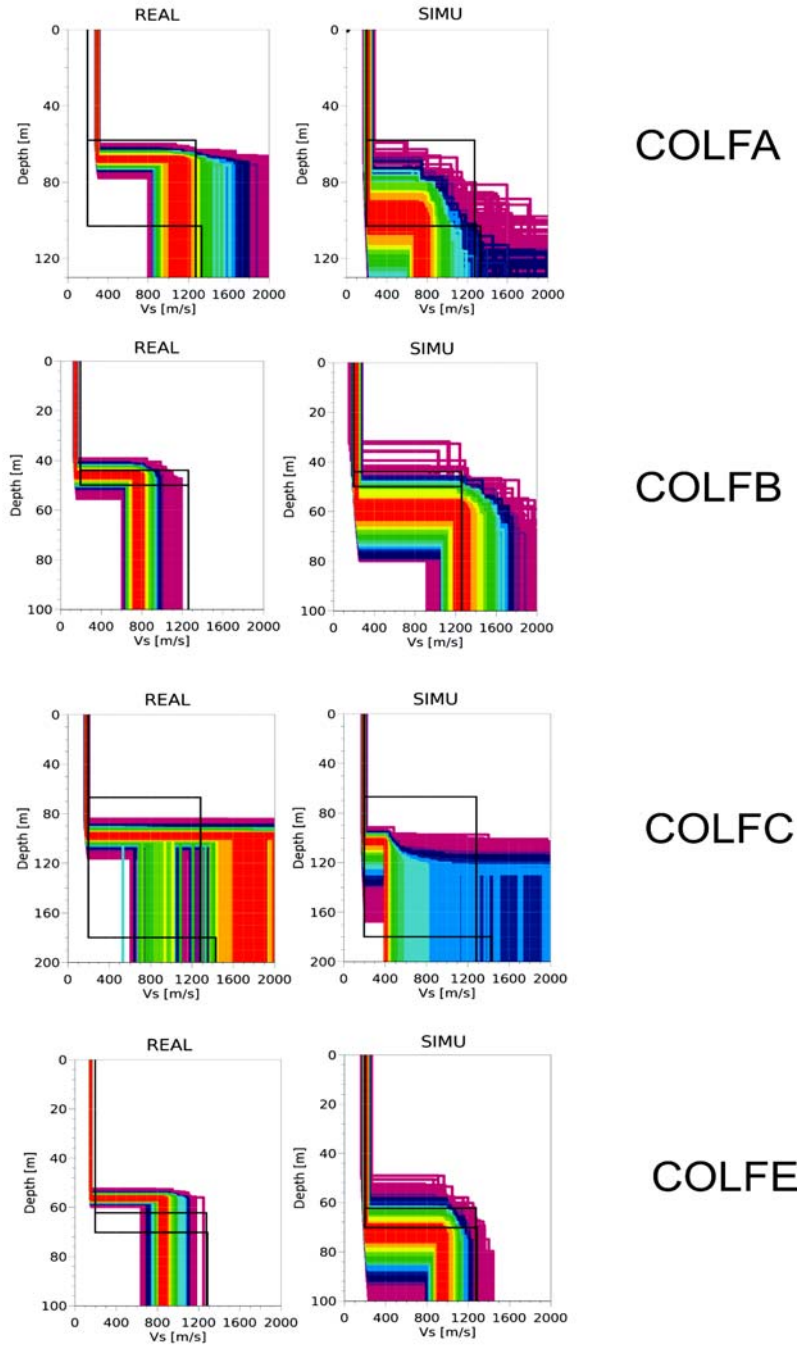


Figure 33 : Inverted S- wave velocities using simulated ambient noise (right panel) and real noise (left panel) for Colfiorito basin. The black lines indicate the velocity profiles related to the minimum and the maximum sediment thickness below the array

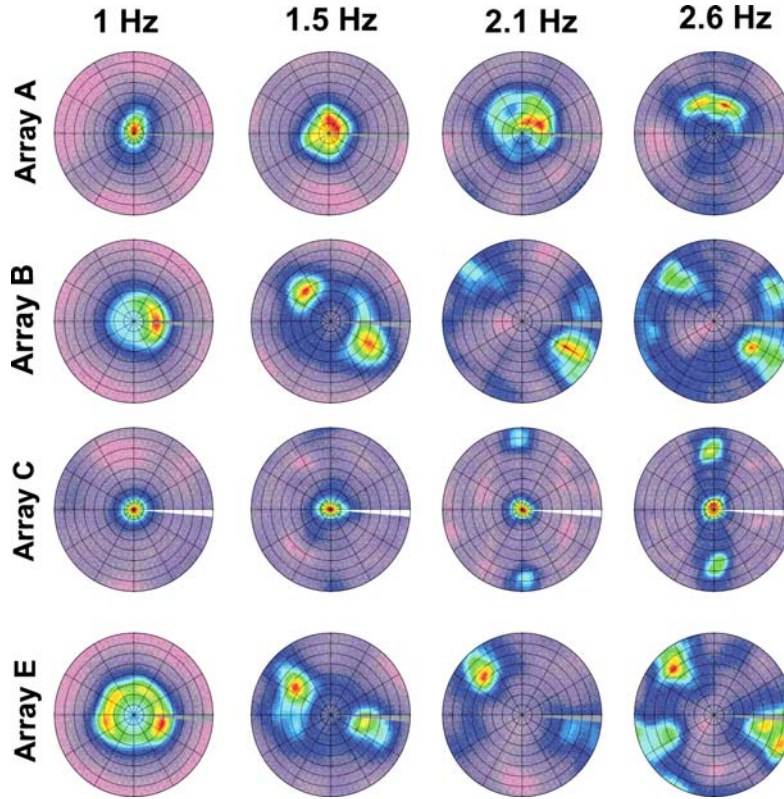


Figure 34: Predominant back-azimuth distribution observed around 4 frequencies (1, 1.5, 2.1 and 2.6 Hz) at the array sites using real noise data. The graphs are normalized to the maximum of the CVFK estimates (red color), and the radial coordinate is proportional to slowness.

6.3.2 Grenoble basin

For the analysis using real noise data, we have considered thirty minutes of ambient noise and used the same parameters as for the array analysis of simulated noise data. As displayed in Figure 35, H/V peak frequencies computed on simulated and real noise are in close agreement. As for simulated noise data, the inversion was performed using a band-limited portion of the dispersion curve from the H/V peak frequency up to 1 Hz. The inverted S-wave velocity profiles using real ambient noise provide the bedrock at a smaller depth (factor of 20% to 30%) than the one given by the inverted S-wave velocity profiles derived from simulated noise data. S-wave velocities estimated within the superficial layers using simulated and real noise data are very close, suggesting thus that the gradient velocity profile used in the noise modeling is on the average reliable. However, phase velocities estimated at Synchrotron and Bon Pasteur sites

are larger than the ones derived from simulated noise data, which may be related to slight lateral variation of the S- wave velocity structure and/or to the misrepresentation of the bedrock topography at the edge of the basin, especially at Synchrotron site.

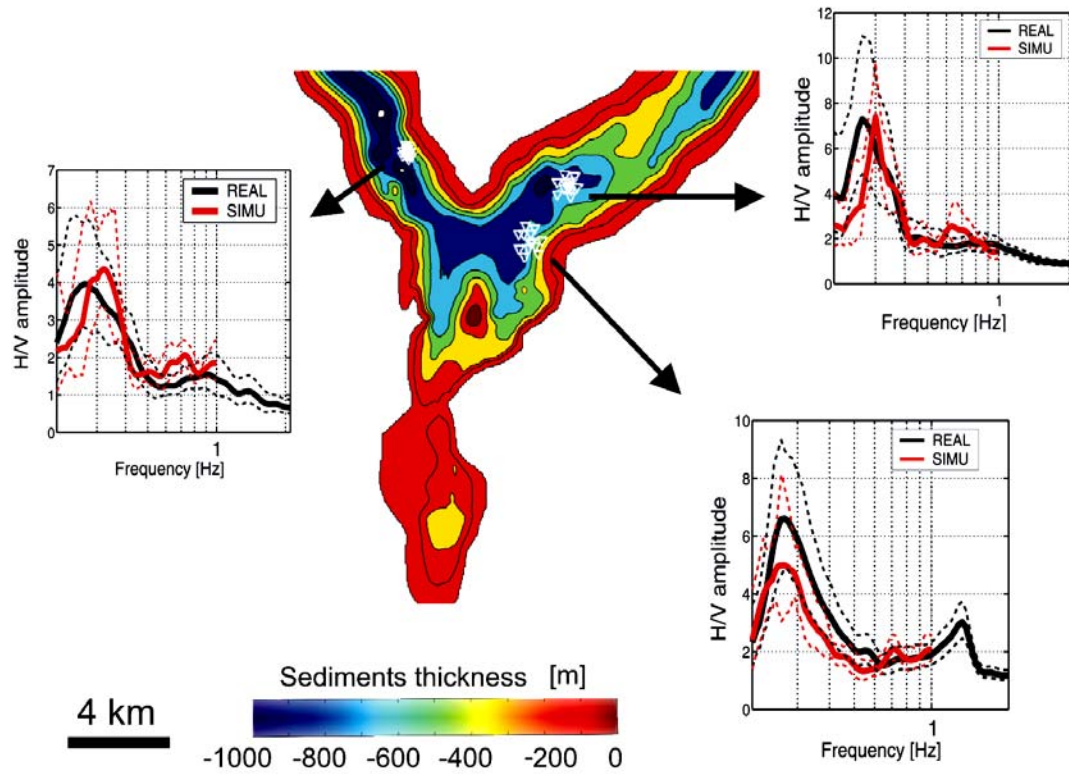


Figure 35: H/V curves computed using simulated (red curves) and real (black curve) noise data

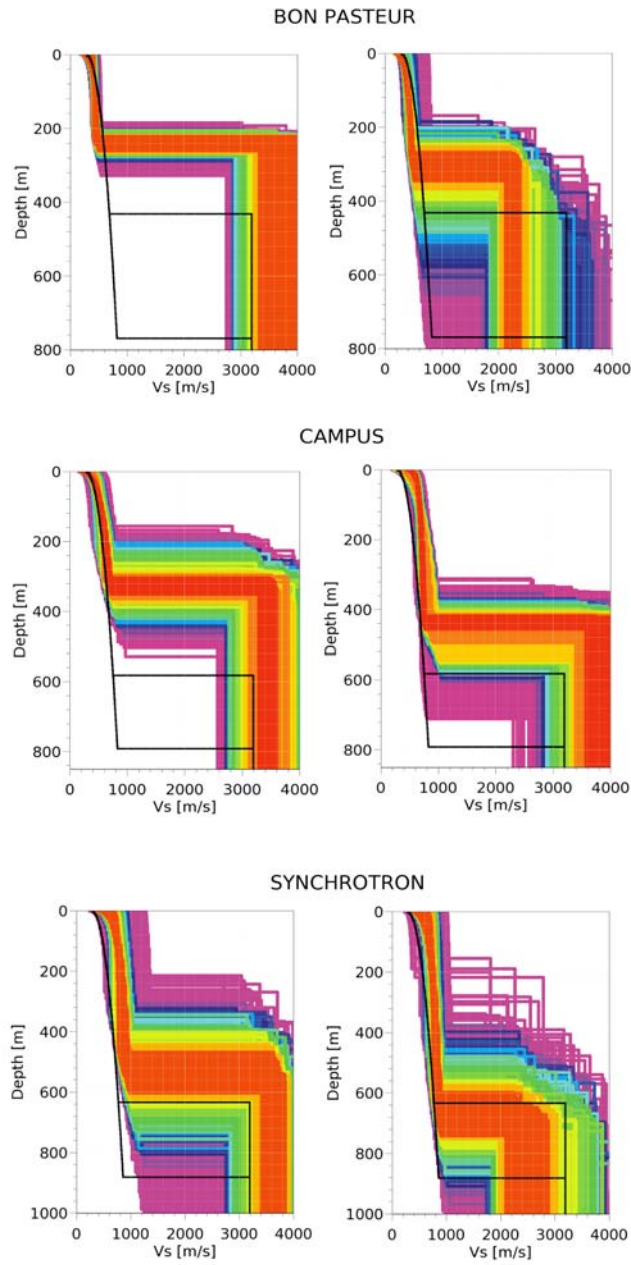


Figure 36: Inverted S- wave velocities using simulated ambient noise (right panel) and real noise (left panel) for Grenoble basin. The black lines indicate the velocity profiles related to the minimum and the maximum sediment thickness below the array

7 Conclusion

The overall good correlation between synthetics and real noise characteristics at the Colfiorito and the Grenoble sites confirm that the modelling of ambient noise as resulting of surface or subsurface forces produced by the human activity is appropriate. Then, the H/V and array analysis applied on simulated noise and the comparison with the real noise measurements for two categories of structures (the Colfiorito basin is a shallow structure, while Grenoble basin is a deep sedimentary structure) have highlighted:

- The capability of H/V technique in mapping the sediment thickness variation. For Colfiorito basin, the H/V frequencies derived from simulated noise are in very close agreement (within 20% at most sites) with the local 1D resonance frequencies. For Grenoble site, the H/V frequencies derived from simulated noise, though significantly differing from the 1D frequencies (overestimation by about 50% in average), exhibit a good correlation with the sediment thickness, and should be closer to the actual 3D resonance frequency of the basin.
- The capability of the array technique in retrieving relevant information about the site velocity structure. When the noise wave field is dominated by 1D wave propagation as it seems so at arrays B and E in Colfiorito, array technique is reliable in providing quantitative information about the soil conditions (S-wave velocity profile and bedrock depth). This capability was also pointed out using simulated noise for simple 1D structures with various velocity profiles (Bonnefoy-Claudet, 2004). For sites exhibiting rapid sediment thickness variation, as it is the case at array A in Colfiorito, the inverted velocity profile seems to be basically related to the average thickness under the array. When the wave field is dominated by 2D/3D wave propagation as for array sites in Grenoble, the array technique doesn't work properly. However, it remains possible to estimate correctly the S-wave velocity corresponding to the higher frequency band of the dispersion curve that involved waves propagating at short enough wavelength in order to be not affected by 2D/3D wave propagation effects.

Finally, the comparison of the H/V peak frequency with the 3D resonance frequency given by the 3D transfer function of the sites should also help in clarifying the discrepancies between H/V and 1D local frequencies, especially for the Grenoble site, and the meaning of the H/V ratio as well as in drawing some practical recommendations when interpreting H/V frequencies for different type of structures. Some further studies have to be conducted using 3D canonical

models in order to better assess the relation between the site geometry and mechanical properties, the wave field properties and the wave velocity profiles obtained using array analysis.

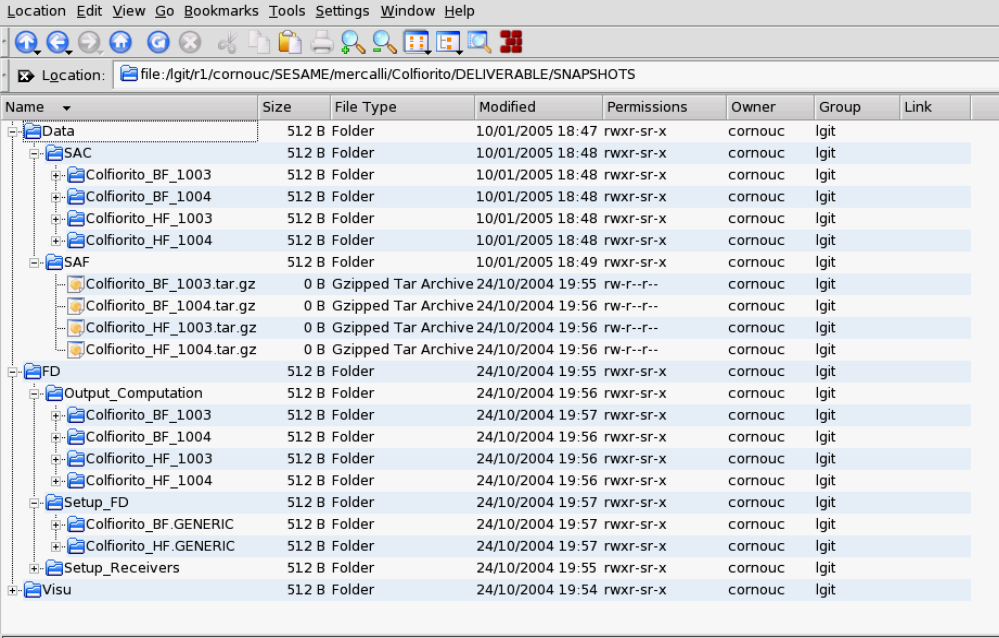
8 Waveform data description

The simulated noise data (around 50 Gbytes) are available in an ftp site accessible on request (mail to Cecile.Cornou@obs.ujf-grenoble.fr). The following informations (Figure 37) are provided:

- All the input files needed for the noise computation (directory **FD/Setup_FD**)
- Information for relating the receivers location in the FD grid with their location in geographical coordinates (directory **FD/Setup_Receivers**), as well as matlab scripts to visualize the model (directory **Visu**)
- Receivers location, source time functions as well as their location and time occurrence (directory **FD/Output_Computation**)
- The FD noise time series in SAC and SAF format after removal of the trend and the mean and fill of the sac header fields (directories **Data/SAC** and **Data/SAF**). These data are ready to be used in CAP software (SESAME Deliverable D18.06).

9 Acknowledgments

This project (Project No. EVG1-CT-2000-00026 SESAME) is supported by the European Commission – Research General Directorate. Most of the computations were performed at the Swiss Center for Scientific Computing (SCSC) and at the Service Commun de Calcul Intensif de l'Observatoire de Grenoble (SCCI). We thank all the personnel from the participating institutions, who have helped in collecting the experimental noise data and in participating to the data archiving and dissemination.



Name	Size	File Type	Modified	Permissions	Owner	Group	Link
Data	512 B	Folder	10/01/2005 18:47	rw-r--r--	cornouc	lgit	
SAC	512 B	Folder	10/01/2005 18:48	rw-r--r--	cornouc	lgit	
Colfiorito_BF_1003	512 B	Folder	10/01/2005 18:48	rw-r--r--	cornouc	lgit	
Colfiorito_BF_1004	512 B	Folder	10/01/2005 18:48	rw-r--r--	cornouc	lgit	
Colfiorito_HF_1003	512 B	Folder	10/01/2005 18:48	rw-r--r--	cornouc	lgit	
Colfiorito_HF_1004	512 B	Folder	10/01/2005 18:48	rw-r--r--	cornouc	lgit	
SAF	512 B	Folder	10/01/2005 18:49	rw-r--r--	cornouc	lgit	
Colfiorito_BF_1003.tar.gz	0 B	Gzipped Tar Archive	24/10/2004 19:55	rw-r--r--	cornouc	lgit	
Colfiorito_BF_1004.tar.gz	0 B	Gzipped Tar Archive	24/10/2004 19:56	rw-r--r--	cornouc	lgit	
Colfiorito_HF_1003.tar.gz	0 B	Gzipped Tar Archive	24/10/2004 19:56	rw-r--r--	cornouc	lgit	
Colfiorito_HF_1004.tar.gz	0 B	Gzipped Tar Archive	24/10/2004 19:56	rw-r--r--	cornouc	lgit	
FD	512 B	Folder	24/10/2004 19:55	rw-r--r--	cornouc	lgit	
Output_Computation	512 B	Folder	24/10/2004 19:56	rw-r--r--	cornouc	lgit	
Colfiorito_BF_1003	512 B	Folder	24/10/2004 19:57	rw-r--r--	cornouc	lgit	
Colfiorito_BF_1004	512 B	Folder	24/10/2004 19:56	rw-r--r--	cornouc	lgit	
Colfiorito_HF_1003	512 B	Folder	24/10/2004 19:56	rw-r--r--	cornouc	lgit	
Colfiorito_HF_1004	512 B	Folder	24/10/2004 19:56	rw-r--r--	cornouc	lgit	
Setup_FD	512 B	Folder	24/10/2004 19:57	rw-r--r--	cornouc	lgit	
Colfiorito_BF_GENERIC	512 B	Folder	24/10/2004 19:57	rw-r--r--	cornouc	lgit	
Colfiorito_HF_GENERIC	512 B	Folder	24/10/2004 19:57	rw-r--r--	cornouc	lgit	
Setup_Receivers	512 B	Folder	24/10/2004 19:55	rw-r--r--	cornouc	lgit	
Visu	512 B	Folder	24/10/2004 19:54	rw-r--r--	cornouc	lgit	

22 Items - 4 Files (0 B Total) - 18 Folders

Figure 37: Organisation of the data

10 References

- Akima, H., A method for bivariate interpolation and smooth surface fitting for irregularly distributed data points, *ACM Transactions on Mathematical Software*, 4, 148-159, 1978.
- Bally, A.W., L. Burbi, C. Cooper, and R. Ghelardoni, Balanced sections and seismic reflection profiles across the central Apennines, *Mem. Soc. Geol. It.*, 35, 257-310, 1986.
- Bard, P.-Y. and Bouchon, M, 1985. The two-dimensional resonance of sediment-filled valleys, *Bull. Seism. Soc. Am.*, 75, 519-541.
- Benton, J., 2004. Etude géotechnique du bassin grenoblois : application au risque sismique, rapport de stage de 3^{ème} année, département géotechnique, Polytech' Grenoble, 75 pages. (in French)
- Bettig B., Bard P-Y, Scherbaum F, Riepl J, Cotton F, Cornou C, Hatzfeld D. "Analysis of dense array noise measurements using the modified spatial auto-correlation method (SPAC): application to the Grenoble area". *Bolettino di Geofisica Teorica ed Applicata* 2001; 42(3-4): 281-304.
- Bitterli-Brunner, P., Fischer, H., 1988. Erläuterungen zum Geologischen Atlas der Schweiz, Blatt Arlesheim (1067), Landeshydrologie- und geologie, Bern.

- Bonnefoy-Claudet S., C. Cornou, M. Ohrnberger, M. Wathelet, P.-Y. Bard, F. Cotton, D. Fäh, 2004. H/V ratio and seismic noise wavefield, EGU 1st General Assembly, Nice, 2004.
- Bonnefoy-Claudet, S., 2004. Nature du bruit de fond sismique : implications pour les études des effets de site, PhD dissertation, Université Joseph Fourier, Grenoble, 216 pp (in French)
- Calamita, F., G. Cello, and G. Deiana, Structural styles, chronology rates of deformations, and time-space relationships in the Umbria-Marche thrust system (central Apennines, Italy), *Tectonics*, 13, 873-881, 1994.
- Cello, G., S. Mazzoli, E. Tondi, and E. Turco, Active tectonics in the Central Apennines and possible implication for seismic hazard analysis in peninsular Italy, *Tectonophysics*, 272, 43-60, 1997.
- Cinti, F., L. Cucci, F. Marra, and P. Montone, The 1997 Umbria-Marche earthquakes (Italy): relations between the surface tectonic breaks and the area of deformation, *Journal of Seismology*, 4, 333-343, 2000.
- Clark (Ed.), S., P., 1966. Handbook of Physical Constants – Revisited Edition, The geological Society of America, Memoir, 1997.
- Cornou, C., 2002, Traitement d'antenne et imagerie sismique dans l'agglomération grenobloise (alpes françaises): implications pour les effets de site, PhD dissertation, Université Joseph Fourier, Grenoble, 260 pp (in French)
- Cornou C, P.-Y. Bard, M. Dietrich, 2003. Contribution of dense array analysis to basin-edge-induced waves identification and quantification. Application to Grenoble basin, French Alps (II), *Bulletin of Seismological Society of America*, 93 , 6, 2624-2648.
- Di Giulio G, Rovelli A, Cara F, Azzara R M, Marra F, Basili R, Caserta A., 2003. Long-duration asynchronous ground motions in the Colfiorito plain, central Italy, observed on a two-dimensional dense array, *Journal of Geophysical Research*, 108(B10), 2486-2500.
- Fäh, D., Rüttener, E., Noack, T., Kruspan, P., 1997. Microzonation of the city of Basel. *Journal of Seismology*, 1, 87-102.
- Gürler, B., Hauber, L. Schwander, M., 1987. Geologie der Umgebung von Basel mit Hinweisen über die Nutzungsmöglichkeiten der Erdwärme, Swiss Geological Commission, N.F. 160, Beitr. geol. Karte Schweiz.
- Kind, F., 2002. Development of Microzonation Methods: Application to Basel, Switzerland. PhD Thesis Nr. 14548, ETH Zuerich.
- Kind, F., Fäh, D., Zechner, E., Huggenberger, P., Giardini, D., 2003. Seismic zonation from a 3D seismic velocity reference model of the area of Basel, Switzerland. *Bull. Seismol. Soc. Am.*, submitted.
- Kind, F., Fäh, D., Giardini, D., 2004. Array measurements of S-wave velocities from ambient vibrations. *Geophysical Journal Int.*, in press.
- Lebrun, B., 1997, Les effets de site: etude expérimentale et simulation de trios configurations, PhD dissertation, Université Joseph Fourier, Grenoble, 208 pp (in French).
- Lebrun, B., D. Hatzfeld, and P.-Y. Bard, 2001, A site effect study in urban area: experimental results in Grenoble (France), *Pageoph.*, 158, 2543-2557.
- Lemeille, F., P.-Y. Bard, F. Cotton, and D. Hatzfeld, "Effet de site sur les ondes sismiques : forage de Montbonnot (Isère) 1. Organisation du projet". Session E4, RST, 17-20 april, 2000

- Meghraoui, M., Delouis, B., Ferry, M., Giardini, D., Huggenberger, P., Spottke, I., Granet, M. 2001. Active Normal Faulting in the Upper Rhine Graben and Paleoseismic Identification of the 1356 Basel Earthquake, *Science*, 293, 2070-2073.
- Messina, P., F. Galadini, P. Galli, and A. Sposato, Quaternary basin evolution and present tectonic regime in the area of the 1997-1998 Umbria-Marche seismic sequence (central Italy), *Geomorphology*, 42, 97-116, 2002.
- Mirabella, F. and S. Pucci, Integration of geological and geophysical data along a section crossing the region of the 1997-1998 Umbria-Marche earthquakes (Italy), *Boll. Soc. Geol. It.*, 1, 891-900, 2002.
- Nakamura Y. "A method for dynamic characteristics estimation of subsurface using microtremor on the ground surface". Quaterly Report Railway Tech. Res. Inst, 1989; 30(1):25-30.
- Nicoud, G., G. Royer, J.-C. Corbin, F. Lemeille, and A. Paillet, 2002. Glacial erosion and infilling of the Isère Valley during the recent Quaternary, *Géologie de la France*, 4, 39-49.
- Noack, T., 1993. Geologische Datenbank der Region Basel, *Eclogae geol. Helv.*, 86, 283-301
- Ohrnberger M., E. Schissele, C. Cornou, S. Bonnefoy-Claudet, M. Wathelet, A. Savvaidis, F. Scherbaum and D. Jongmans, 2004a. Frequency wavenumber and spatial autocorrelation methods for dispersion curve determination from ambient vibration recordings. Proceedings of the 13th World Conference on Earthquake Engineering. Vancouver, Canada, August 1-6, Paper 946
- Ohrnberger M., E. Schissele, C. Cornou, M. Wathelet, A. Savvaidis, F. Scherbaum, D. Jongmans and F. Kind, 2004b. Microtremor array measurements for site effect investigations: comparison of analysis methods for field data crosschecked by simulated wavefields. Proceedings of the 13th World Conference on Earthquake Engineering. Vancouver, Canada., August 1-6, Paper 940.
- Roten D., C. Cornou, S. Steimen, D. Fäh, D. Giardini, 2004. 2D resonances in alpine valleys from ambient vibration wavefields, 13th World Conference on Earthquake Engineering, Vancouver, Canada, August 1-6, paper 845.
- Rovelli, A., L. Scognamiglio, F. Marra, and A. Caserta, Edge-diffracted 1-s surface waves observed in a small-size intermontane basin (Colfiorito, central Italy), *Bull. Seism. Soc.Am.*, 91, 1851-1866, 2001.
- Scherbaum, F., J. Riepl, B. Bettig, M. Ohrnberger, C. Cornou, F. Cotton, P.-Y. Bard, 1999. Dense array measurements of ambient vibrations in the Grenoble basin to study local site effects, AGU Fall meeting, San Francisco, December 1999.
- SESAME Deliverable D09.02, "FD code to generate noise synthetics", SESAME EVG1-CT-2000-00026 project, 31 pages, 2002.
- SESAME Deliverable D08.02, "Measurement guidelines", SESAME EVG1-CT-2000-00026 project, 96 pages, 2002
- SESAME Deliverable D18.06, "User manual for software package CAP - a continuous array processing toolkit for ambient vibration array analysis". SESAME EVG1-CT-2000-00026 project, 83pp, 2004.
- SESAME Deliverable D13.08, "Nature of noise wavefield", SESAME EVG1-CT-2000-00026 project, 50 pages, 2004.

- Steimen, S., 1999. 2-D Resonanzen in der Mulde von St. Jacob Tullingen. Diplomarbeit ETH Zürich.
- Steimen, S., D. Fäh, F. Kind, C. Schmid and D. Giardini, 2003. Identifying 2-D Resonance in Microtremor Wave Fields, *Bull. Seism. Soc. Am.*, 93, 583 – 599.
- Tokimatsu K, 1997. Geotechnical site characterization using surface waves, Ishihara, Editors. *Earthquake Geotechnical Engineering*. Rotterdam:AA Balkema, 1333-1368.
- Vallon, M., 1999, Estimation de l'épaisseur d'alluvions et sédiments quaternaires dans le région grenobloise par inversion des anomalies gravimétriques, IRSN/CNRS Internal Report, 34 pp (in French)
- Wathelet, M, D. Jongmans D, and M. Ohrnberger, 2004. Surface wave inversion using a direct search algorithm and its application to ambient vibrations measurements. *Near Surface Geophysics*, *in press*
- Zechner, E., Kind, F., Fäh, D., Huggenberger, P., 2001. 3-D Geological Modell of the Southern Rhinegraben compiled on existing geological data and geophysical reference modeling., Abstract Volume of the 2nd EUCOR-URGENT Workshop, 7.-11. October, Mont Saint-Odile, Strasbourg, France, 43pp.

11 List of Figures

- Figure 1: Thickness of the low-velocity layer in map view. (a) normal faults; (b) thrust faults; (c) anticline axes; (d) syncline axes; (e) borehole location; (f) geophysical survey lines. After Di Giulio et al. [2003] 8
- Figure 2: P- and S- wave velocities derived from down-hole measurements [A. Rovelli, *personal communication*] 9
- Figure 3: Arrays distribution within the Colfiorito basin (left panel) and configuration of the arrays (right panel) deployed during the 2002 measurement campaign. 10
- Figure 4: Topography of the low-velocity layer, with the receivers (black dots) and the sources (white dots) locations. 11
- Figure 5: a) Grenoble basin's digital elevation model and, superimposed, the 3D contour map of the basement's depth (white lines) inferred from gravimetric measurements (Vallon, 1999). Depth is given in meters. Location of the array and the borehole are also indicated. b) P- (thick line) and S- (thin line) wave interval velocity profiles derived from vertical and offset seismic profiles measurements at the borehole location (Cornou, 2002)..... 13
- Figure 6: Contour map of the basement's depth (black lines) inferred from gravimetric measurements (red triangles). After Vallon (1999)..... 14
- Figure 7: Seismic profiles (Vertical and offset seismic profiles, seismic refraction and reflection profiles) performed nearby the borehole location (after Cornou, 2002) 15

Figure 8: (A) Array distribution within the city of Grenoble. The array locations are denoted by letters A-I. Arrays A and H as well as E and D occupied nearly the same locations with different apertures. (B) Array design. Apertures: A: 121 m; B : 122 m ; C : 143 m ; D : 169 m ; F : 584 m ; G : 192 m ; H : 1001 m. After Scherbaum et al. (1999).	17
Figure 9: (left) Approximative geographical array location. (right) Outer and inner array configuration. The BP00 station is located at the center of the inner array.....	18
Figure 10: 2004 H/V noise measurements campaign. Measured points are indicated by the yellow star. After Benton (2004).	18
Figure 11: Interval P- and S- wave velocity (black squares) at the borehole location and interpolated P- (blue line) and S- (red line) velocities.....	19
Figure 12: Topography of the low-velocity layer, receivers (black dots) and sources (white dots) location.....	20
Figure 13: Geologic 3D model geometry (Zechner et al., 2001). Through the transparent topography with contours the geologic units below the surficial Quaternary sediments can be seen (labels as defined in Table 7). Between the red bottom layer and the topography the seismic contrast layer is visible in yellow. The faults included in the model are partially visible as blue shade. Blue drilling rig symbols indicate deep boreholes from which information was available. A red line indicates the limits of the Canton of Basel for orientation.	22
Figure 14 : Overview of the data sources for seismic velocities available for the model (Kind, 2002).	24
Figure 15: Measured versus calculated fundamental frequencies from the model before the corrections to the geology. The dotted range marks the uncertainty margin in the measured frequencies. Part a) shows the values calculated with the average S-wave velocity model, while part b) shows the values calculated with the maximum S-wave velocities as crosses and circles for the minimal S-wave velocity models (from Kind, 2002).....	26
Figure 16: Magnitude of the corrections applied to the model geometry at the bottom of the Meletta layer in meters. Positive values indicate an increase of the thickness, negative values a decrease. Crosses mark the location of deep boreholes constraining the deeper interfaces (from Kind, 2002).	27
Figure 17: Illustration of the corrections to the geologic model proposed by Kind (2002). The upper part of the figure shows a section from the initial model, while the lower part of the figure shows the same section after the correction. The labeled structures are the Allschwil fault zone (AF), the horst of Basel (HB), the syncline of St. Jacob Tüllingen and the Tabular Jura (TJ). A triangle and a dash dotted line indicate the area of the horst of Basel where the new borehole confirmed the corrections to the model geometry.....	29
Figure 18: Measured versus calculated fundamental frequencies from the corrected geometrical model. The measured f_0 (thick gray line) is shown sorted by value with the gray shaded area indicating the uncertainty from the interpretation of the H/V ratios. The thin black lines show the calculated f_0 and the uncertainty range in the calculations derived from the uncertainty in the S-wave velocity model (Kind, 2002).	29
Figure 19: H/V (triangles) and array (filled circles) measurements within the Basel area (after Kind, 2002). The topography is indicated in gray scale.	31

Figure 20: Array geometries at the three measured sites within the SESAME project (SESAME Deliverable D06.05)	32
Figure 21: Topography of the bedrock, receivers (black dots) and sources (white dots) location	33
Figure 22: Topography of the layers given in Table 9. Distances are given in the Swiss coordinates system.....	34
Figure 23: Noise simulation for Colfiorito basin: (a) contouring display of the 1D resonance frequencies estimated at each receiver location; (b) contouring display of the H/V peak frequency; (c) relative deviation of the H/V peak frequencies from the 1D resonance frequencies; (d) H/V peak frequency as a function of the 1D resonance frequency, the 1:1 relative deviation from the 1D resonance frequency is indicated by the thick black line, the 20% and 40% deviation are indicated by the thick and thin dashed lines, respectively.	38
Figure 24: Noise simulation for Grenoble basin: (a) contouring display of the 1D resonance frequencies estimated at each receiver location; (b) contouring display of the H/V peak frequency; (c) relative deviation of the H/V peak frequencies from the 1D resonance frequencies; (d) H/V peak frequency as a function of the 1D resonance frequency, the 1:1 relative deviation from the 1D resonance frequency is indicated by the thick black line, the 20% and 40% deviation are indicated by the thick and thin dashed lines, respectively.	39
Figure 25: (left) topography of the low-velocity layer and array geometry (black dots); (right) depth of the bedrock below each receiver. The white dots for COLFC array indicate receivers that were not used in the array analysis. See Figure 3 for the arrays location within the basin.....	41
Figure 26: Noise simulation for Colfiorito basin: inverted P- and S- wave velocities and measured dispersion curves (black dots) for Colfiorito basin. The black lines indicate the velocity profiles related to the minimum and the maximum sediment thickness below the array. See Figure 3 for the arrays location within the basin.	42
Figure 27: Dispersion curves estimated using simulated noise data (black dots) and real noise data (green dots). The red lines indicate the dispersion curves of the fundamental Rayleigh waves mode computed using 1D soil profiles that correspond to the maximum, minimum and average sediment thickness below the array.	43
Figure 28: (left) topography of the low-velocity layer and array geometry; (right) depth of the bedrock below each receiver	45
Figure 29: Noise simulation for Grenoble basin: inverted P- and S- wave velocities and measured dispersion curves (black dots) for Grenoble basin. The black lines indicate the velocity profiles related to the minimum and the maximum sediment thickness below the array.....	46
Figure 30: Dispersion curves estimated using simulated noise data (black dots) and real noise data (green dots). The red lines indicate the dispersion curves of the fundamental Rayleigh waves mode computed using 1D soil profiles that corresponds to the maximum, minimum and average sediment thickness below the array.	47
Figure 31: Inverted P- and S- wave velocities for the theoretical dispersion curve of the fundamental Rayleigh waves mode indicated in the right panel (black dots). The black lines indicate the velocity profiles used for the computation of the theoretical dispersion curve.	47

Figure 32: H/V curves computed using simulated (red curves) and real (black curve) noise data	49
Figure 33 : Inverted S- wave velocities using simulated ambient noise (right panel) and real noise (left panel) for Colfiorito basin. The black lines indicate the velocity profiles related to the minimum and the maximum sediment thickness below the array	50
Figure 34: Predominant back-azimuth distribution observed around 4 frequencies (1, 1.5, 2.1 and 2.6 Hz) at the array sites using real noise data. The graphs are normalized to the maximum of the CVFK estimates (red color), and the radial coordinate is proportional to slowness.....	51
Figure 35: H/V curves computed using simulated (red curves) and real (black curve) noise data	52
Figure 36: Inverted S- wave velocities using simulated ambient noise (right panel) and real noise (left panel) for Grenoble basin. The black lines indicate the velocity profiles related to the minimum and the maximum sediment thickness below the array	53
Figure 37: Organisation of the data	56

12 List of Tables

Table 1: Geophysical parameters of the Colfiorito basin considered for the noise simulation	11
Table 2: Noise simulation performed for the Colfiorito basin	11
Table 3: Computation parameters used for Colfiorito model	12
Table 4: Geophysical parameters for the Grenoble basin.....	20
Table 5: Simulation parameters for the Grenoble basin	20
Table 6: List of computations for the Grenoble basin	20
Table 7: Stratigraphic units represented in the 3D-model and their abbreviations.	22
Table 8: Geophysical parameters of the 3D model (Kind, 2002; Kind et al., 2003, 2004)..	24
Table 9: Geophysical parameters for the Basel basin.....	35
Table 10 : Simulation parameters for the Basel modeling	36
Table 11 : List of computation for the Basel model	36